Multicasting in Stochastic MIMO Networks

Youngmin Jeong, *Student Member, IEEE*, Tony Q. S. Quek, *Senior Member, IEEE*,
Jin Sam Kwak, *Member, IEEE*, and Hyundong Shin, *Senior Member, IEEE*

***Abstract*—Physical-layer multicast transmission, which seeks to deliver information messages to all users simultaneously, is becoming more important in wireless systems with demand for various multimedia mobile applications such as Multimedia Broadcast Multicast Services. The spatial randomness of communicating nodes in a wireless network is one of inevitable uncertainties in the design and analysis of network information flow and connectivity. The use of multiple antennas at both transmitting and receiving nodes is the most promising strategy to increase spectral efficiency and communication reliability as well as to enhance physical-layer confidentiality of wireless systems. In this paper, we characterize multicasting in such a stochastic multiple-input multiple-output (MIMO) network where a probe transmitter broadcasts confidential data with *sectorized transmission* to legitimate receivers sitting in a region $\mathcal{R}$. We first put forth a measure of the total amount of information flow, called the *space–time capacity*, into $\mathcal{R}$ in a spatial random field of legitimate receivers without accounting for intrinsic confidentiality at the physical layer. We then derive the space–time capacity into the sectoral region $\mathcal{R}$ and the nth nearest ergodic capacity in a Poisson field to characterize the spatial average and ordering of MIMO ergodic capacity achieved by legitimate receivers in $\mathcal{R}$. Using the Marčenko–Pastur law, we further assess the asymptotic space–time capacity and the nth nearest ergodic capacity per receive antenna as the antenna numbers tend to infinity. In the presence of eavesdropping, we determine a total amount of confidential information flow per receive antenna, called the *space–time secrecy rate*, into $\mathcal{R}$ in Poisson fields of receiving equivalents—with asymptotic arguments. Using an asymptotic secrecy graph on $\mathcal{R}$, we also characterize *local* confidential connectivity such as the secrecy range, out-degree, and out-isolation probability of the probe transmitter. The framework developed in this work enables us to quantify the local information flow in random MIMO wireless networks by averaging first small-scale fading processes *over time* and then large-scale path losses *over space*.**

***Index Terms*—Broadcast, confidential connectivity, ergodic capacity, multicast, multiple-input multiple-output (MIMO), physical-layer security, Poisson network, random matrix theory, secrecy rate, stochastic geometry.**

Manuscript received August 1, 2012; revised March 11 and October 11, 2013; accepted January 7, 2014. The associate editor coordinating the review of this paper and approving it for publication was S. Affes.

This paper was presented in part at the IEEE Global Communications Conference, Anaheim, CA, December 2012, and the IEEE International Conference on Communications, Budapest, Hungary, June 2013. This work was supported, in part, by the Basic Science Research Program through the National Research Foundation of Korea (NRF) funded by the Ministry of Science, ICT and Future Planning (2009-0083495), and NRF-2011-220-D00076 by the Ministry of Education, and the SRG ISTD 2012037.

Y. Jeong and H. Shin are with the Department of Electronics and Radio Engineering, Kyung Hee University, 1732 Deogyeong-daero, Giheung-gu, Yongin-si, Gyeonggi-do, 446-701 Korea (e-mail: hshin@khu.ac.kr). H. Shin is the corresponding author.

T. Q. S. Quek is with the Singapore University of Technology and Design, and the Institute for Infocomm Research, Singapore.

J. S. Kwak is with the WILUS Institute of Standards and Technology, 263-2 Yangjae-dong, Seocho-gu, Seoul 137-894, Korea.

Digital Object Identifier 10.1109/TWC.2014.022214.121108

I. Introduction

THE design of physical-layer multicast transmission has been of interest for a wide range of wireless applications such as Multimedia Broadcast Multicast Services [1]–[3]. Such multicast transmission conveys information to a multicast group (subscribers) simultaneously. Moreover, the multicast transmission must guarantee reliable data transmission to all users: the information has to be retransmitted to all the users when any user fails to receive the correct information. As part of efficient radio resource management in such a multicast system, a large wave of work has been spawned on the design of multicast systems and the analysis of information-theoretic limits for wireless multicast networks (see, e.g., [4]–[15] and references therein). In particular, multiple-antenna transmission is one of enabling technologies to improve the performance of multicast systems [11]–[15].

In single-rate multicasting, all users receive data at the same rate and the multicast connection is bottlenecked by the worst channel-gain user in order to minimize outage and retransmission. However, responding to calls from *heterogeneous* users in real-time applications such as teleconferencing, video streaming, and distance learning, it is desirable to serve each user in the multicast group at a rate commensurate with its own demand and max-flow capability. As one solution for such multirate multicasting, the use of multiple description coding (MDC) enables us to divide source data into equally-important multiple substreams, called descriptions, such that any subset of the descriptions can be used to decode the original data stream and a better quality is achieved by more descriptions [16], [17]. For example, in muticarrier wireless systems such as orthogonal frequency division multiplexing, the MDC allows flexibility in multicasting to heterogeneous users together with intelligent subcarrier allocation [9]. Another approach for multirate multicast is to use multi-resolution codes, giving hierarchical data descriptions to allow decoding at a variety of rates with progressive refinement [18].

In the last decade, the extensive work on multiple-input multiple-output (MIMO) systems has spurred to integrate this technology into existing and emerging wireless networks such as the IEEE 802.11n wireless local area network (WLAN), IEEE 802.16 WiMAX, and 3GPP Long Term Evolution (Advanced) [19]–[22]. The linear scaling of information flow or channel capacity with the number of antennas is well understood for MIMO systems in rich-scattering wireless environments and it is well known that multiple antennas can be exploited to realize the multiplexing gain, diversity gain, and/or array gain (for interference suppression). Therefore, the use of multiple antennas at both transmitting and receiving nodes is the most promising solution to increase spectral efficiency and reliability in wireless communication [23]–

[31]. The broadcast nature of the wireless medium, however, makes wireless networks vulnerable to eavesdropping by adversarial nodes. Hence, communication confidentiality is a fundamental issue in such wireless networks. Shannon laid the early foundations on the information-theoretic security to reinforce eavesdropper's uncertainty (equivocation) about messages [32]—followed by Wyner [33]. An intrinsically secure network aims to deliver messages reliably to the legitimate node(s), while minimizing information leakage to the eavesdropping node(s) [34]. By exploiting the stochastic randomness of a underlying broadcast channel, the use of multiple antennas is again an attractive strategy to enhance physical-layer confidentiality of wireless systems [35]–[41]. In particular, it has been shown that a rank-one input covariance matrix (i.e., *beamforming*) is optimal for the secrecy capacity of a multiple-input single-output wiretap channel [35, Theorem 2]. For a MIMO wiretap channel, the input covariance optimization for the secrecy capacity was independently stated in [36, Theorem 1] and [37, Theorem 1].[1] It was also proved that without knowing channel states of the eavesdropper, positive secrecy rates can be guaranteed using multiple antennas [41].

In addition to wireless propagation, the spatial randomness of communicating nodes in a wireless network is one of inevitable uncertainties in the design and analysis of network information flow and connectivity. Since the geometry of node locations determines a desired or interfering signal power at each receiving node, it plays a key role in networking behavior. Therefore, spatial modeling of wireless networks in terms of stochastic geometry [42], [43] is essential for establishing a unified framework to characterize the *spatial average* of network performances in a probabilistic way. In this framework, a wireless network at time instant is treated as a snapshot of a stationary random field of communicating nodes in Euclidean space, where the locations of network nodes are viewed as the realizations of point processes. In particular, Poisson models have been extensively used to describe spatial node distributions in diverse wireless networks to characterize, for example: network interference, the number of successful radio transceivers (or transmission capacity), secure connectivity, and secrecy rates [44]–[53]. Hence, we are motivated to evaluate information flow and confidential connectivity in MIMO multicast networks on both *spatial and temporal average*.

In this paper, we consider a stochastic MIMO multicast network, where a *probe* transmitter broadcasts confidential messages with *sectorized transmission* to legitimate receivers sitting in a region $\mathcal{R}$ in the presence of passive eavesdroppers (without jamming and colluding). All the nodes in the network are equipped with multiple antennas. Specifically, we embody the spatial randomness of receiving nodes (legitimate receivers and eavesdroppers) according to Poisson point processes (PPPs) in characterizing *local* information flow into the region $\mathcal{R}$ with or without accounting for communication confidentiality at the physical layer. The main contributions of the paper can be summarized as follows.

- In the absence of eavesdropping, we first introduce a measure of the total amount of information flow—called the *space–time capacity*—into the region $\mathcal{R}$ in a spatial random field of legitimate receivers by averaging first small-scale fading processes over time and then large-scale path losses over space (see Definition 1). We then derive the space–time capacity into the sectoral region $\mathcal{R}$ in a Poisson field of legitimate receivers (see Proposition 1); and characterize the spatial ordering of MIMO ergodic capacity achieved by legitimate receivers sitting in $\mathcal{R}$ in terms of the ergodic capacity of a communication channel between the probe transmitter and its nth nearest receiver (see Proposition 2). Using the Marčenko–Pastur law [54], [55], we further assess the asymptotic space–time capacity and the nth nearest ergodic capacity per receive antenna as the antenna numbers at both the transmitter and the receiver tend to infinity (see Propositions 3 and 4).
- In the presence of eavesdropping, we define a measure of the total amount of confidential information flow per receive antenna—called the *space–time secrecy rate*—into the region $\mathcal{R}$ against the most adversarial eavesdropper in spatial random fields of receiving nodes, as the antenna numbers of the transmitter, legitimate receiver, and eavesdropper go to infinity (see Definition 3). Applying Campbell's theorem [42], [43] and the Shannon transform of the Marčenko–Pastur law [55], we represent the space–time secrecy rate for a unbounded sectoral region $\mathcal{R}$ in Poisson fields (see Proposition 5). It is unveiled that the information leakage to the eavesdroppers is negligible as the growing rate of the antenna number at the receiver increases and/or the growing rate at the eavesdropper decreases.
- Using the asymptotic secrecy graph on $\mathcal{R}$ (see Definition 2), we characterize local confidential connectivity such as: i) the secrecy range (i.e., the maximum range of confidential connection with a positive secrecy rate), ii) the out-degree (i.e., the number of legitimate receivers in $\mathcal{R}$ securely connected to the transmitter), and iii) the out-isolation probability (i.e., the probability that the transmitter is not securely connected to any legitimate receivers in $\mathcal{R}$). When the antenna numbers of the legitimate receivers and eavesdroppers grow at the *same rate*, the secrecy range is equal to the distance of the nearest eavesdropper from the transmitter; the out-degree is equal to $\lambda_{\rm r}/\lambda_{\rm e}$; and the out-isolation probability is equal to $\lambda_{\rm e}/\left(\lambda_{\rm r}+\lambda_{\rm e}\right)$ for the spatial density $\lambda_{\rm r}$ of legitimate receivers and $\lambda_{\rm e}$ of eavesdroppers.

The rest of the paper is organized as follows. In Section II, we present the system model. The local information flow in Poisson MIMO multicast networks is analyzed in Section III. Numerical examples are provided in Section IV and conclusions are finally given in Section V. The notation and symbols used in the paper are tabulated in Table I. We also adopt the convention of using letters without serifs for random variables.

II. System Model

We consider a stochastic MIMO multicast network, as illustrated in Fig. 1. An $n_{\rm t}$-antenna transmitter (Alice) broadcasts

[1] See, e.g., [40] for the equivalence between these two optimization formulations.

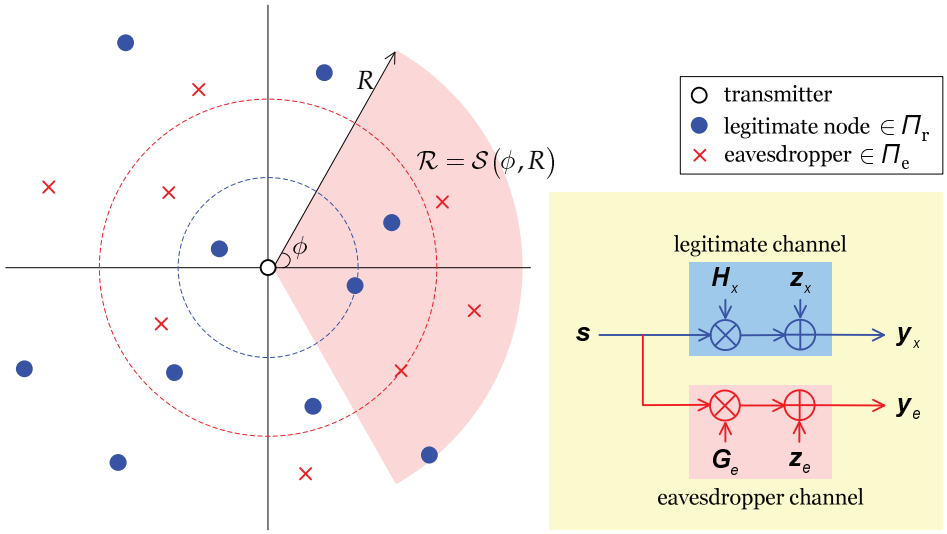

Fig. 1. A stochastic MIMO multicast network with the sectoral transmission region $\mathcal{R} = \mathcal{S}(\phi, R)$, Poisson field Π_r of legitimate receivers, and Poisson field Π_e of eavesdroppers.

confidential messages to n_r-antenna legitimate receivers (the Bobs) randomly located in a two-dimensional region in the presence of n_e-antenna potential eavesdroppers (the Eves) randomly scattered again in space.[2]

A. Spatial Node Distributions

The probe transmitter is *deterministically* located at the origin of the coordinate system. Since node positions are unknown to network designers *a priori*, the legitimate receivers and eavesdroppers are assumed to be scattered according to independent homogeneous PPPs $\Pi_r(\lambda_r)$ and $\Pi_e(\lambda_e)$ in the two-dimensional plane $\mathbb{R}^2$. Therefore, for a legitimate receiver or eavesdropper being inside the region $\mathcal{R}$, its spatial location is conditionally uniform over $\mathcal{R}$. A homogeneous PPP $\Pi(\lambda)$ is characterized by the single parameter λ, which we use to denote the spatial density of nodes (i.e., the number of nodes per unit area). The probability of k nodes being in the region $\mathcal{R}$ is given by [42], [43]

$$\mathbb{P}\{k \text{ nodes in } \mathcal{R}\} = e^{-\lambda|\mathcal{R}|}\frac{(\lambda|\mathcal{R}|)^k}{k!}, \qquad k \in \mathbb{Z}_+ \tag{1}$$

where $|\mathcal{R}|$ denotes the area of $\mathcal{R}$. The PPP is a simple and persuasive model for node locations in the network where the node positions are completely random [44]–[53]. This model was also verified by experiments in a network with mobility [53].

B. Signal and Channel Models

The channel state information (CSI) is assumed to be perfectly available at receiving nodes (legitimate receivers and eavesdroppers). Let $\boldsymbol{H}_x \sim \tilde{\mathcal{N}}_{n_r,n_t}(\mathbf{0}, \mathbf{I}_{n_r}, \mathbf{I}_{n_t})$ and $\boldsymbol{G}_e \sim \tilde{\mathcal{N}}_{n_e,n_t}(\mathbf{0}, \mathbf{I}_{n_e}, \mathbf{I}_{n_t})$ be $n_r \times n_t$ and $n_e \times n_t$ Rayleigh (small-scale) fading channel matrices from the transmitter to a typical legitimate receiver located at x and an typical eavesdropper at e in $\mathcal{R}$, respectively.[3] We further assume that the probe transmitter knows the location information of both the legitimate receivers and eavesdroppers in $\mathcal{R}$. Then, the received signal vectors at the receiver x and the eavesdropper e can be written respectively as

$$\boldsymbol{y}_x = |x|^{-\alpha/2}\boldsymbol{H}_x\boldsymbol{s} + \boldsymbol{z}_x \tag{2}$$

$$\boldsymbol{y}_e = |e|^{-\alpha/2}\boldsymbol{G}_e\boldsymbol{s} + \boldsymbol{z}_e \tag{3}$$

where $\boldsymbol{s}$ is the $n_t \times 1$ transmitted signal vector with the power constraint $\mathbb{E}\{\|\boldsymbol{s}\|^2\} \le P$; $\boldsymbol{z}_x \sim \tilde{\mathcal{N}}_{n_r,1}(\mathbf{0}, \sigma^2\mathbf{I}_{n_r}, 1)$ and $\boldsymbol{z}_e \sim \tilde{\mathcal{N}}_{n_r,1}(\mathbf{0}, \sigma^2\mathbf{I}_{n_e}, 1)$ are zero-mean additive white Gaussian noise vectors at the receiver x and the eavesdropper e, respectively; and $\alpha \ge 2$ is a power loss exponent. We denote the average transmit SNR by $\gamma = P/\sigma^2$. In what follows, we refer to $p = \min(n_r, n_t)$, $q = \max(n_r, n_t)$, and define a random matrix $\boldsymbol{W}_x \in \mathbb{C}^{p\times p}$ as

$$\boldsymbol{W}_x \triangleq \begin{cases} \boldsymbol{H}_x\boldsymbol{H}_x^\dagger, & \text{if } n_r \le n_t \\ \boldsymbol{H}_x^\dagger\boldsymbol{H}_x, & \text{otherwise.} \end{cases} \tag{4}$$

Then, $\boldsymbol{W}_x$ is the complex central Wishart matrix $\tilde{\mathcal{W}}_p(q, \mathbf{I}_p)$ [23].

III. MIMO Multicasting

As shown in Fig. 1, we deal with a sectorized transmission, where the transmission becomes *omnidirectional* if the sectoring angle ϕ is equal to π. A transmission strategy is chosen adaptively depending on network design purposes (e.g., broadcast, multicast, and routing). In particular, the sectorized transmission has been well studied, for example, to increase communication confidentiality at the physical layer [51], [52] and ad-hoc network throughput [59].

[2]The framework developed in this work can be extended in a straightforward way to an arbitrary space dimension.

[3]The fading processes of all links are assumed to be ergodic and independent.

A. Space–Time Capacity

Let us first consider local information flow in the absence of eavesdroppers (i.e., $\lambda_{\rm e}=0$) or transmission of messages into the region $\mathcal{R}$ without accounting for confidentiality. We begin by introducing a measure of the total amount of information flow into $\mathcal{R}$, which captures both spatial (large-scale) and temporal (small-scale) averages of achievable rates. The spatial average is made over all the collections (the probability space) of node locations in the region $\mathcal{R}$ described by a subset of point processes.

Definition 1 (Space–Time Capacity into $\mathcal{R}$): The space–time capacity in nats/s/Hz into $\mathcal{R}$ in a spatial random field Ψ of legitimate receivers, denoted by $\mathcal{C}(\mathcal{R})$, is defined as

$$\mathcal{C}(\mathcal{R}) \triangleq \mathbb{E}_{\Psi,\boldsymbol{H}_x}\left\{\sum_{x\in\Psi\cap\mathcal{R}}\frac{1}{\Delta_{\rm r}}\ln\det\left(\mathbf{I}_{n_{\rm r}}+\frac{\gamma}{n_{\rm t}\left|x\right|^{\alpha}}\boldsymbol{H}_x\boldsymbol{H}_x^{\dagger}\right)\right\} \tag{5}$$

where $\Delta_{\rm r}$ is a multicast degree of freedom.

Remark 1: The space–time capacity $\mathcal{C}(\mathcal{R})$ measures a total amount of information transfer to legitimate receivers in $\mathcal{R}$ by averaging first small-scale fading processes (i.e., $\boldsymbol{H}_x$) over time and then large-scale (distant-dependent) path losses (i.e., $|x|^{-\alpha}$) over space. Operationally, the time averaging is achieved from coding across many coherence time intervals of ergodic fading processes, whereas the space averaging is made over point processes of node locations. Note that this measure is akin to the multicast throughput in [7, Definition 1] and [9, eq. (2)], defined as the sum of the throughputs provided the base station to each individual user within the multicast system.

Remark 2: The multicast degree of freedom $\Delta_{\rm r}$ accounts for multirating and/or scheduling in multicast. We remark its choice as follows:

- For $\Delta_{\rm r}=1$, $\mathcal{C}(\mathcal{R})$ can be interpreted as a upper bound on the average throughput of any multicast scheduling scheme (e.g., the worst-, best-, and median-user schedulers) [6]–[8] or multirate multicast without paying attention to the rate bottleneck of slow receivers [9].
- For the finite region ($R<\infty$) with

$$\Delta_{\rm r}=\mathbb{E}\left\{\sum_{x\in\Psi}\mathbb{1}\left\{x\in\mathcal{R}\right\}\right\}=\lambda_{\rm r}R^2\phi, \tag{6}$$

  $\mathcal{C}(\mathcal{R})$ gives the ergodic sum capacity for multicasting to the receivers in the region $\mathcal{R}=\mathcal{S}(\phi,R)$ with uniform scheduling.
- For the infinite region ($R\to\infty$) with $\Delta_{\rm r}=N$, $\mathcal{C}(\mathcal{R})$ gives a upper bound on the ergodic sum capacity for multicasting to the N nearest receivers with uniform scheduling since $\Delta_{\rm r}\mathcal{C}(\mathcal{R})$ quickly saturates to a constant value as $R\to\infty$ (see Remark 3 and Fig. 3).

Property 1: Let $\Psi=\Pi(\lambda)$ and $\mathcal{R}=\mathcal{S}(\phi,R)$ be a circular sector with opening angle 2ϕ and radius R. Then, we have

$$\begin{aligned}&\mathbb{E}_{\Psi}\left\{\sum_{x\in\Psi\cap\mathcal{R}}\ln\left(1+c\left|x\right|^{-\alpha}\right)\right\}\\&\overset{\rm (a)}{=}\lambda\int_0^{2\phi}\int_0^{R}r\ln\left(1+cr^{-\alpha}\right)drd\theta\\&\overset{\rm (b)}{=}\lambda\phi\Bigg[\pi c^{\frac{2}{\alpha}}\csc\left(\frac{2\pi}{\alpha}\right)+R^2\ln\left(1+cR^{-\alpha}\right)\\&\qquad+\frac{\alpha cR^{2-\alpha}}{(2-\alpha)}\,{}_2F_1\left(1,1-\frac{2}{\alpha};2-\frac{2}{\alpha};-cR^{-\alpha}\right)\Bigg]\end{aligned} \tag{7}$$

where c is an arbitrary positive constant; (a) follows from Campbell's theorem [42]; and (b) is obtained with the help of [56, eqs. (2.728.1) and (3.194.1)] by making the change of variable $r^{-\alpha}=t$. Note that the Slivnyak–Mecke theorem states that the reduced Palm distribution of the PPP is equal to its original distribution [43]. Hence, we can remove the origin (location of the transmitter) from the receiver process and treat $\Pi_{\rm r}\setminus\{0\}$ instead of $\Pi_{\rm r}$ to avoid the singular receiver location

$$\begin{aligned}\mathcal{C}(\mathcal{R})=\frac{\lambda_{\rm r}\phi}{\Delta_{\rm r}}\sum_{i=0}^{p-1}\sum_{j=0}^{i}\sum_{\ell=0}^{2j}\Bigg[&\frac{(-1)^{\ell}(2j)!\binom{2i-2j}{i-j}\binom{2j+2q-2p}{2j-\ell}}{2^{2i-\ell}j!\ell!(q-p+j)!}\Bigg\{\pi\csc\left(\frac{2\pi}{\alpha}\right)\left(\frac{\gamma}{n_{\rm t}}\right)^{\frac{2}{\alpha}}\Gamma\left(1+m+\frac{2}{\alpha}\right)\\&+R^2m!e^{\zeta}\sum_{k=0}^{m}E_{k+1}(\zeta)+\frac{\alpha R^2}{\zeta(2-\alpha)}(m+1)!\zeta^{\frac{\alpha-2}{2\alpha}}e^{\zeta/2}W_{\frac{2-\alpha}{2\alpha},\frac{1}{\alpha}}(\zeta)\Bigg\}\Bigg]\end{aligned} \tag{9}$$

$$\begin{aligned}\mathcal{C}(\mathcal{R})&=\mathbb{E}_{\Psi}\left\{\sum_{x\in\Psi\cap\mathcal{R}}\frac{1}{\Delta_{\rm r}}\mathbb{E}_{\boldsymbol{W}_x}\left\{\ln\det\left(\mathbf{I}_p+\frac{\gamma}{n_{\rm t}\left|x\right|^{\alpha}}\boldsymbol{W}_x\right)\right\}\right\}\\&=\frac{1}{\Delta_{\rm r}}\sum_{i=0}^{p-1}\sum_{j=0}^{i}\sum_{\ell=0}^{2j}\frac{(-1)^{\ell}(2j)!\binom{2i-2j}{i-j}\binom{2j+2q-2p}{2j-\ell}}{2^{2i-\ell}j!\ell!(q-p+j)!}\int_0^{\infty}\mathbb{E}_{\Psi}\left\{\sum_{x\in\Psi\cap\mathcal{R}}\ln\left(1+\frac{\gamma z}{n_{\rm t}\left|x\right|^{\alpha}}\right)\right\}z^{q-p+\ell}e^{-z}dz\end{aligned} \tag{10}$$

$$\Delta_{\rm r}\mathcal{C}(\mathcal{R})=\lambda_{\rm r}\pi\phi\left(\frac{\gamma}{n_{\rm t}}\right)^{\frac{2}{\alpha}}\csc\left(\frac{2\pi}{\alpha}\right)\sum_{i=0}^{p-1}\sum_{j=0}^{i}\sum_{\ell=0}^{2j}\frac{(-1)^{\ell}(2j)!\binom{2i-2j}{i-j}\binom{2j+2q-2p}{2j-\ell}\Gamma\left(1+q-p+\ell+\frac{2}{\alpha}\right)}{2^{2i-\ell}j!\ell!(q-p+j)!} \tag{11}$$

TABLE I
NOTATION AND SYMBOLS

$(\cdot)^{\dagger}$	Transpose conjugate
$[x]^{+}$	Positive part of x: $[x]^{+}=\max(x,0)$
$\mathbb{C}$	Complex numbers
$\mathbb{R}$	Real numbers
$\mathbb{R}_{+}$	Nonnegative real numbers
$\mathbb{Z}_{+}$	Nonnegative integers
$\mathbb{1}\{\cdot\}$	Indicator function
$\mathbf{I}_n$	$n\times n$ identity matrix
$\mathbb{E}\{\cdot\}$	Expectation operator
$\mathbb{P}\{\cdot\}$	Probability measure
$p_X(x)$	Probability density function of X
$F_X(x)$	Cumulative distribution function of X
$\xrightarrow{\text{a.s.}}$	Almost sure convergence
$\Pi(\lambda)$	Two-dimensional Poisson point process with intensity λ: we simply denote it by Π if the intensity λ is apparent.
$\tilde{\mathcal{N}}_{m,n}(\boldsymbol{M},\boldsymbol{\Sigma},\boldsymbol{\Psi})$	$m\times n$ matrix-variate complex Gaussian distribution [23, Definition II.1]
$\tilde{\mathcal{W}}_m(n,\boldsymbol{\Sigma})$	$m\times m$ complex central Wishart distribution [23, Definition II.1]
$\mathsf{Rayleigh}(\sigma)$	Rayleigh distribution with parameter σ: $p_X(x)=\frac{x}{\sigma^2}\exp\left(-\frac{x^2}{2\sigma^2}\right),\ x\geq 0$
$\mathcal{S}(\phi,R)$	Circular sector with opening angle 2ϕ
$\delta(z)$	Dirac's delta function
$\Gamma(\cdot)$	Euler's Gamma function: $\Gamma(z)=\int_0^{\infty}t^{z-1}\exp(-t)\,dt$
${}_2F_1(a,b;c;z)$	Gauss hypergeometric function [56, eq. (9.14.2)]
$E_n(z)$	Exponential integral function of order n: $E_n(z)=\int_1^{\infty}e^{-zx}x^{-n}dx$, $n=0,1,2,\ldots,\ \Re(z)>0$
$W_{\lambda,\nu}(z)$	Whittaker function [56, eq. (9.220.4)]
$G_{p,q}^{m,n}(\cdot)$	Meijer's G-function [57, eq. (8.2.1.1)]
$H_{p,q}^{m,n}[\cdot]$	Fox's H-function [57, eq. (8.3.1.1)]
$H_{\mathcal{M},(p_1:p_2),\mathcal{N},(q_1:q_2)}^{\mathcal{L},n_1,n_2,m_1,m_2}[\cdot]$	Fox's H-function of two variables [58, eq. (2.2.1)]

for a distance. As $R\to\infty$, the second and third terms in (7) vanish for this unbounded sectoral region $\mathcal{R}=\mathcal{S}(\phi,\infty)$, leading to

$$\mathbb{E}_{\Psi}\left\{\sum_{x\in\Psi\cap\mathcal{R}}\ln\left(1+c\,|x|^{-\alpha}\right)\right\}=\lambda\phi\pi c^{\frac{2}{\alpha}}\csc\left(\frac{2\pi}{\alpha}\right). \quad (8)$$

Proposition 1 (Space–Time Capacity in a Poisson Field): Let $\Psi=\Pi_{\mathrm{r}}$. Then, the space–time capacity $\mathcal{C}(\mathcal{R})$ in nats/s/Hz into $\mathcal{R}=\mathcal{S}(\phi,R)$ for the sectorized transmission is given by (9), where $m=q-p+\ell$ and $\zeta=n_{\mathrm{t}}R^{\alpha}/\gamma$.

Proof: Using [23, eq. (47)], we have (10). Using Property 1 and evaluating the integral with the help of [23, eq. (47)], [56, eq. (3.381.4)], and [57, eq. (2.21.2.2)], we complete the proof. □

Remark 3: The space–time capacity $\mathcal{C}(\mathcal{R})$ is *strictly proportional* to both the spatial density of receivers and the sectoring angle ϕ. As $R\to\infty$, (9) reduces by using (8) to (11).

B. Spatial Ordering of Ergodic Capacity

We now determine the ergodic capacity of a MIMO link between the transmitter and its nth nearest legitimate receiver in $\mathcal{R}$ to characterize the spatial ordering of MIMO ergodic capacity in $\mathcal{R}$. In what follows, we consider a unbounded sectoral region $\mathcal{R}=\mathcal{S}(\phi,\infty)$ since the contributions of legitimate receivers far from the transmitter to total regional (or local) information flow are negligible due to large path losses (see Fig. 3 for example). Let $\{x_n\}$ be a random (location) set of legitimate receivers sitting in $\mathcal{R}$ in ascending order of the distance from the probe transmitter at the origin (i.e., $|x_1|<|x_2|<|x_3|<\cdots$) and R_n denote the distance $|x_n|$ of the nth nearest receiver. Then, the nth nearest distance R_n for the unbounded sectoral region $\mathcal{R}=\mathcal{S}(\phi,\infty)$ follows the generalized Gamma distribution:[4]

$$p_{R_n}(r)=e^{-\lambda_{\mathrm{r}}\phi r^2}\frac{2\left(\lambda_{\mathrm{r}}\phi r^2\right)^n}{r\Gamma(n)},\qquad r\geq 0. \quad (12)$$

In particular, the nearest distance is distributed as $R_1\sim\mathsf{Rayleigh}\left(1/\sqrt{2\lambda_{\mathrm{r}}\phi}\right)$.

Proposition 2 (The nth Nearest Ergodic Capacity): Let $\Psi=\Pi_{\mathrm{r}}$ and $\mathcal{R}=\mathcal{S}(\phi,\infty)$. Then, the ergodic capacity in nats/s/Hz of a MIMO link between the probe transmitter and its nth nearest receiver in $\mathcal{R}$ is given by (13).

Proof: Using again [23, eq. (43)], we have

$$\langle C\rangle_n(\mathcal{R})=\frac{1}{\Delta_{\mathrm{r}}}\sum_{i=0}^{p-1}\sum_{j=0}^{i}\sum_{\ell=0}^{2j}\left\{\frac{(-1)^{\ell}(2j)!\binom{2i-2j}{i-j}\binom{2j+2q-2p}{2j-\ell}}{2^{2i-\ell}j!\ell!(q-p+j)!}\times\underbrace{\int_0^{\infty}\mathbb{E}_{R_n}\left\{\ln\left(1+\frac{\gamma z}{n_{\mathrm{t}}R_n^{\alpha}}\right)\right\}}_{\triangleq\mathcal{I}}z^{q-p+\ell}e^{-z}dz\right\}. \quad (14)$$

To evaluate the integral $\mathcal{I}$, we make the change of variable $\frac{\gamma z}{n_{\mathrm{t}}r^{\alpha}}=y$, leading to

$$\mathcal{I}=\frac{2}{\alpha\Gamma(n)}\left(\frac{\gamma z\left(\lambda_{\mathrm{r}}\phi\right)^{\frac{\alpha}{2}}}{n_{\mathrm{t}}}\right)^{\frac{2n}{\alpha}}\times\int_0^{\infty}\ln(1+y)\,e^{-\lambda_{\mathrm{r}}\phi\left(\frac{n_{\mathrm{t}}y}{\gamma z}\right)^{-\frac{2}{\alpha}}}y^{-\frac{2n+\alpha}{\alpha}}dy. \quad (15)$$

We express $\ln(1+y)$ and $e^{-\lambda_{\mathrm{r}}\phi\left(\frac{n_{\mathrm{t}}y}{\gamma z}\right)^{-2/\alpha}}$ in terms of Fox's H-functions with the help of [57, eq. (8.4.6.5)] and [58, eq. (1.7.2)] as follows:

$$\ln(1+y)=H_{2,2}^{1,2}\left[y\,\middle|\,\begin{matrix}(1,1),(1,1)\\(1,1),(0,1)\end{matrix}\right] \quad (16)$$

$$e^{-\lambda_{\mathrm{r}}\phi\left(\frac{n_{\mathrm{t}}y}{\gamma z}\right)^{-\frac{2}{\alpha}}}=\frac{\alpha}{2}H_{0,1}^{1,0}\left[\left(\lambda_{\mathrm{r}}\phi\right)^{\frac{\alpha}{2}}\frac{\gamma z}{n_{\mathrm{t}}y}\,\middle|\,\begin{matrix}-\\(0,\frac{\alpha}{2})\end{matrix}\right]. \quad (17)$$

Substituting (16)–(17) into (15) and using the Mellin transform of the product of two Fox's H-functions [58, eq. (2.6.8)], we

[4]It follows again from the mapping theorem that the sequence $\{R_n^2\}$ for $\mathcal{R}=\mathcal{S}(\phi,\infty)$ represents Poisson arrivals on the line $\mathbb{R}_+$ with the arrival rate $\lambda_{\mathrm{r}}\phi$ and R_n^2 has the Erlang distribution of order n with rate $\lambda_{\mathrm{r}}\phi$ [52].

get

$$\mathcal{I} = \frac{1}{\Gamma(n)} H_{2,3}^{2,2}\left[\frac{\gamma z\left(\lambda_{\mathrm{r}}\phi\right)^{\frac{\alpha}{2}}}{n_{\mathrm{t}}}\,\middle|\,\begin{matrix}(1,1),(1,1)\\ \left(n,\frac{\alpha}{2}\right),(1,1),(0,1)\end{matrix}\right]. \tag{18}$$

Finally, substituting (18) into (14), expressing e^{-z} in terms of the Fox's H-function with the help of [57, eq. (8.4.3.1)], and using again the Mellin transform of two Fox's H-functions, we arrive at the desired result. □

Example 1 (Standard Network): When $\alpha = 2$ or more generally, the power loss exponent α is equal to the network spatial dimension (called the *standard network*), the nth nearest ergodic capacity reduces to (19).

Remark 4: For $\Delta_{\mathrm{r}} = 1$, the nth nearest ergodic capacity can be interpreted as the ergodic unicast capacity with opportunistic transmission scheduling. Furthermore, letting $\Delta_{\mathrm{r}} = n$, the nth nearest ergodic capacity gives the exact ergodic sum capacity for multicast transmission to the n nearest receivers with uniform multicast scheduling.

C. Asymptotic Analysis

As a counterpart to the Wishart distribution for finite dimensional random matrices, another key result in random matrix theory states that as the matrix dimensions grow, the empirical distribution of eigenvalues for a large class of random matrices converges almost surely to a nonrandom limiting distribution. More specifically to MIMO systems, as the antenna numbers n_{r} and n_{t} tend to infinity in such a way that $n_{\mathrm{t}}/n_{\mathrm{r}} \to \tau$, the empirical density of the eigenvalues of $n_{\mathrm{r}}^{-1}\boldsymbol{H}_x\boldsymbol{H}_x^{\dagger}$ converges almost surely to the so-called Marčenko–Pastur density [54], [55]:

$$f^{\star}(z;\tau) = [1-\tau]^{+}\delta(z) + \frac{\sqrt{[z-a_\tau]^{+}[b_\tau - z]^{+}}}{2\pi z} \tag{20}$$

where $a_\tau = \left(1-\sqrt{\tau}\right)^2$ and $b_\tau = \left(1+\sqrt{\tau}\right)^2$. We now characterize the local information flow in the stochastic MIMO multicast network with large-scale antenna configurations.

Lemma 1: The Mellin transform of the Marčenko–Pastur density $f^{\star}(z;\tau)$ in (20) is given by

$$\begin{aligned}\mathcal{M}_{\mathrm{mp}}(s;\tau) &\triangleq \int_0^{\infty} z^{s-1} f^{\star}(z;\tau)\,dz\\ &= \frac{b_\tau^s}{16}\left(\frac{b_\tau - a_\tau}{b_\tau}\right)^2 {}_2F_1\left(2-s,\frac{3}{2};3;\frac{b_\tau-a_\tau}{b_\tau}\right).\end{aligned} \tag{21}$$

Proof: By making the change of variable $z - a_\tau = y$, we have

$$\mathcal{M}_{\mathrm{mp}}(s;\tau) = \frac{1}{2\pi}\int_0^{b_\tau - a_\tau} (y+a_\tau)^{s-2}\sqrt{y(b_\tau - a_\tau - y)}\,dy. \tag{22}$$

Then, with the help of [56, eq. (3.197.8)] and [57, eq. (7.3.1.3)], we complete the proof. □

Proposition 3: Let

$$\mathcal{C}^{\star}(\mathcal{R};\tau) \triangleq \lim_{\substack{n_{\mathrm{t}},n_{\mathrm{r}}\to\infty\\ n_{\mathrm{t}}/n_{\mathrm{r}}\to\tau}} \frac{\mathcal{C}(\mathcal{R})}{n_{\mathrm{r}}} \tag{23}$$

be the asymptotic space–time capacity per receive antenna into $\mathcal{R}$. Then, for the Poisson field of receivers $\Psi = \Pi_{\mathrm{r}}$ and the sectorized transmission $\mathcal{R} = \mathcal{S}(\phi,\infty)$, we have

$$\begin{aligned}\mathcal{C}^{\star}(\mathcal{R};\tau) = \frac{\lambda_{\mathrm{r}}\phi\pi}{16\Delta_{\mathrm{r}}}\left(\frac{b_\tau\gamma}{\tau}\right)^{\frac{2}{\alpha}}\csc\left(\frac{2\pi}{\alpha}\right)\frac{(b_\tau-a_\tau)^2}{b_\tau}\\ \times {}_2F_1\left(1-\frac{2}{\alpha},\frac{3}{2};3;\frac{b_\tau-a_\tau}{b_\tau}\right).\end{aligned} \tag{24}$$

Proof: Using (20), the asymptotic space–time capacity $\mathcal{C}^{\star}(\mathcal{R},\tau)$ can be written as

$$\begin{aligned}&\mathcal{C}^{\star}(\mathcal{R};\tau)\\ &= \mathbb{E}_{\Psi}\left\{\sum_{x\in\Psi\cap\mathcal{R}}\frac{1}{\Delta_{\mathrm{r}}}\int_{a_\tau}^{b_\tau}\ln\left(1+\frac{\gamma z}{\tau|x|^{\alpha}}\right)f^{\star}(z;\tau)\,dz\right\}\\ &= \frac{\lambda_{\mathrm{r}}\phi\pi}{\Delta_{\mathrm{r}}}\left(\frac{\gamma}{\tau}\right)^{\frac{2}{\alpha}}\csc\left(\frac{2\pi}{\alpha}\right)\mathcal{M}_{\mathrm{mp}}\left(1+\frac{2}{\alpha};\tau\right)\end{aligned} \tag{25}$$

where the last equality follows from Property 1. Finally, using Lemma 1, we arrive at the desired result. □

Remark 5: Note that $\mathcal{C}^{\star}(\mathcal{R},\tau)$ is a monotonically increasing function in $\tau \geq 0$. As $\tau \to \infty$, $n_{\mathrm{t}}^{-1}\boldsymbol{H}_x\boldsymbol{H}_x^{\dagger}$ converges almost surely to $\mathbf{I}_{n_{\mathrm{r}}}$ by the law of large numbers and hence,

$$\frac{1}{n_{\mathrm{r}}}\ln\det\left(\mathbf{I}_{n_{\mathrm{r}}} + \frac{\gamma}{n_{\mathrm{t}}|x|^{\alpha}}\boldsymbol{H}_x\boldsymbol{H}_x^{\dagger}\right) \xrightarrow{\text{a.s.}} \ln\left(1+\gamma|x|^{-\alpha}\right). \tag{26}$$

It follows from (8) and (26) that

$$\mathcal{C}^{\star}(\mathcal{R};\infty) = \frac{\lambda_{\mathrm{r}}\phi\pi}{\Delta_{\mathrm{r}}}\gamma^{\frac{2}{\alpha}}\csc\left(\frac{2\pi}{\alpha}\right), \tag{27}$$

which is the maximum scaling of the space–time capacity into

$$\langle C\rangle_n(\mathcal{R}) = \frac{1}{\Delta_{\mathrm{r}}\Gamma(n)}\sum_{i=0}^{p-1}\sum_{j=0}^{i}\sum_{\ell=0}^{2j}\frac{(-1)^{\ell}(2j)!\binom{2i-2j}{i-j}\binom{2j+2q-2p}{2j-\ell}}{2^{2i-\ell}j!\ell!(q-p+j)!}H_{3,3}^{2,3}\left[\frac{\gamma\left(\lambda_{\mathrm{r}}\phi\right)^{\frac{\alpha}{2}}}{n_{\mathrm{t}}}\,\middle|\,\begin{matrix}(1,1),(1,1),(-q+p-\ell,1)\\ \left(n,\frac{\alpha}{2}\right),(1,1),(0,1)\end{matrix}\right] \tag{13}$$

$$\langle C\rangle_n(\mathcal{R}) = \frac{1}{\Delta_{\mathrm{r}}\Gamma(n)}\sum_{i=0}^{p-1}\sum_{j=0}^{i}\sum_{\ell=0}^{2j}\frac{(-1)^{\ell}(2j)!\binom{2i-2j}{i-j}\binom{2j+2q-2p}{2j-\ell}}{2^{2i-\ell}j!\ell!(q-p+j)!}G_{3,3}^{2,3}\left(\frac{\gamma\lambda_{\mathrm{r}}\phi}{n_{\mathrm{t}}}\,\middle|\,\begin{matrix}1,1,-q+p-\ell\\ n,1,0\end{matrix}\right) \tag{19}$$

$\mathcal{R}$ with the receive antennas.

Proposition 4: Let $\Psi = \Pi_{\mathrm{r}}$, $\mathcal{R} = \mathcal{S}(\phi, \infty)$, and

$$C_n^\star(\mathcal{R};\tau) \triangleq \lim_{\substack{n_{\mathrm{t}},n_{\mathrm{r}}\to\infty \\ n_{\mathrm{t}}/n_{\mathrm{r}}\to\tau}} \frac{\langle C\rangle_n(\mathcal{R})}{n_{\mathrm{r}}} \tag{28}$$

be the asymptotic ergodic capacity per receive antenna of a MIMO link between the probe transmitter and its nth nearest receiver in $\mathcal{R}$. Then, the nth nearest asymptotic ergodic capacity in nats/s/Hz per receive antenna is given by (29).

Proof: Using again (20), we have

$$C_n^\star(\mathcal{R};\tau) = \mathbb{E}_{R_n}\left\{\frac{1}{\Delta_{\mathrm{r}}}\int_{a_\tau}^{b_\tau} \ln\left(1+\frac{\gamma z}{\tau R_n^\alpha}\right) f^\star(z;\tau)\,dz\right\}. \tag{30}$$

It follows from (18) that

$$\begin{aligned} &C_n^\star(\mathcal{R};\tau) \\ &= \frac{1}{2\pi\Delta_{\mathrm{r}}\Gamma(n)}\int_{a_\tau}^{b_\tau}\left\{\frac{1}{z}\sqrt{(z-a_\tau)(b_\tau-z)}\right. \\ &\left.\times H_{2,3}^{2,2}\left[\frac{\gamma z(\lambda_{\mathrm{r}}\phi)^{\frac{\alpha}{2}}}{\tau}\,\middle|\,\begin{matrix}(1,1),(1,1)\\ \left(n,\frac{\alpha}{2}\right),(1,1),(0,1)\end{matrix}\right]dz\right\}. \end{aligned} \tag{31}$$

Using the fractional integral of Fox's H-function [60, eq. (2.75)], we complete the proof. □

Remark 6: Similar to (27), as $\tau\to\infty$, we have

$$\begin{aligned} &C_n^\star(\mathcal{R};\infty) \\ &= \mathbb{E}_{R_n}\left\{\frac{1}{\Delta_{\mathrm{r}}}\ln\left(1+\gamma R_n^{-\alpha}\right)\right\} \\ &= \frac{1}{\Delta_{\mathrm{r}}\Gamma(n)}H_{2,3}^{2,2}\left[\gamma(\lambda_{\mathrm{r}}\phi)^{\frac{\alpha}{2}}\,\middle|\,\begin{matrix}(1,1),(1,1)\\ \left(n,\frac{\alpha}{2}\right),(1,1),(0,1)\end{matrix}\right]. \end{aligned} \tag{32}$$

D. Space–Time Secrecy Rate

In this subsection, we characterize local confidential information flow in stochastic MIMO multicast networks using asymptotic arguments. The secure communication problem has been typically addressed at the upper layers in which confidential messages are scrambled by cryptographic protocols that are computationally hard for the adversary to decipher: e.g., Secure Shell (SSH) at the application layer, Internet Protocol Security (IPsec) at the network layer, and Wi-Fi Protected Access (WPA) at the link layer. In contrast to this computational security, the physical-layer security for transmission of confidential messages aims at exploiting inherent randomness of physical medium such as channel noises and channel fluctuations due to fading. The MIMO advantage to this form of intrinsic security has been recently discovered in analogy with the spatial multiplexing gain, thereby the fading is beneficial for secrecy capacity [35]–[40].

Definition 2 (Asymptotic Secrecy Graph on $\mathcal{R}$): The asymptotic secrecy graph on $\mathcal{R}$ in spatial random fields Ψ of legitimate receivers and Ω of eavesdroppers is defined as the directed random graph $\mathcal{G}(\mathcal{R}) = \{\Psi, \mathcal{E}\}$ with the vertex set Ψ and the edge set

$$\mathcal{E} = \left\{\overrightarrow{ox} : \mathcal{R}_{\mathrm{s}}^\star(x,\Omega,\tau,\eta) > 0,\ x\in\Psi\cap\mathcal{R}\right\} \tag{33}$$

where $\mathcal{R}_{\mathrm{s}}^\star(x,\Omega,\tau,\eta)$ is the asymptotic secrecy rate per receive antenna achieved by the legitimate receiver $x\in\Pi_{\mathrm{r}}$ in $\mathcal{R}$, given by (34).[5]

Definition 3 (Space–Time Secrecy Rate into $\mathcal{R}$): The space–time secrecy rate into $\mathcal{R}$ in spatial random fields Ψ of legitimate receivers and Ω of eavesdroppers, denoted by $i\mathcal{S}(\mathcal{R};\tau,\eta)$, is defined as

$$i\mathcal{S}(\mathcal{R};\tau,\eta) \triangleq \mathbb{E}_{\Psi,\Omega}\left\{\frac{1}{\Delta_{\mathrm{s}}}\sum_{x\in\Psi\cap\mathcal{R}}\mathcal{R}_{\mathrm{s}}^\star(x,\Omega,\tau,\eta)\right\} \tag{35}$$

where Δ_{s} is a multicast degree of freedom for secure transmission.

Remark 7: The space–time secrecy rate $i\mathcal{S}(\mathcal{R};\tau,\eta)$ measures a total amount of confidential information flow per receive antennas into legitimate receivers in $\mathcal{R}$ against the most adversarial eavesdropper, as n_{t}, n_{r}, and n_{e} go to infinity in such a way that $n_{\mathrm{t}}/n_{\mathrm{r}}\to\tau$ and $n_{\mathrm{r}}/n_{\mathrm{e}}\to\eta$. Since the Gramian matrices of small-scale fading ($\boldsymbol{H}_x$ and $\boldsymbol{G}_e$) behave as nonrandom quantities when the antenna numbers grow infinitely large, it is obvious that the eavesdropper nearest to

[5]Note that $\mathcal{G}(\mathcal{R})$ and $\mathcal{R}_{\mathrm{s}}^\star(x,\Omega)$ are asymptotic versions of the $i\mathcal{S}$-graph [51, Definition 2.2] and the maximum secrecy rate [51, eq. (2)], respectively, as the antenna numbers tend to infinity. This $i\mathcal{S}$-graph model does not make assumptions concerning availability of full CSI [51].

$$C_n^\star(\mathcal{R};\tau) = \frac{(b_\tau-a_\tau)^2}{4\sqrt{\pi}a_\tau\Delta_{\mathrm{r}}\Gamma(n)}\,H_{1,(3:1),0,(3:2)}^{1,2,1,2,1}\left[\begin{matrix}\dfrac{\tau}{\gamma a_\tau(\lambda_{\mathrm{r}}\phi)^{\frac{\alpha}{2}}} \\ \dfrac{b_\tau}{a_\tau}-1\end{matrix}\,\middle|\,\begin{matrix}(0,1)\\ \hline \left(1-n,\frac{\alpha}{2}\right),(0,1),(1,1);\left(-\frac{1}{2},1\right)\\ (0,1),(0,1),(0,1);(0,1),(-2,1)\end{matrix}\right] \tag{29}$$

$$\mathcal{R}_{\mathrm{s}}^\star(x,\Omega,\tau,\eta) \triangleq \min_{e\in\Omega\cap\mathcal{R}}\left[\lim_{\substack{n_{\mathrm{t}},n_{\mathrm{r}},n_{\mathrm{e}}\to\infty \\ n_{\mathrm{t}}/n_{\mathrm{r}}\to\tau \\ n_{\mathrm{r}}/n_{\mathrm{e}}\to\eta}}\frac{\ln\det\left(\mathbf{I}_{n_{\mathrm{r}}}+\frac{\gamma}{n_{\mathrm{t}}|x|^\alpha}\boldsymbol{H}_x\boldsymbol{H}_x^\dagger\right)-\ln\det\left(\mathbf{I}_{n_{\mathrm{e}}}+\frac{\gamma}{n_{\mathrm{t}}|e|^\alpha}\boldsymbol{G}_e\boldsymbol{G}_e^\dagger\right)}{n_{\mathrm{r}}}\right]^+ \tag{34}$$

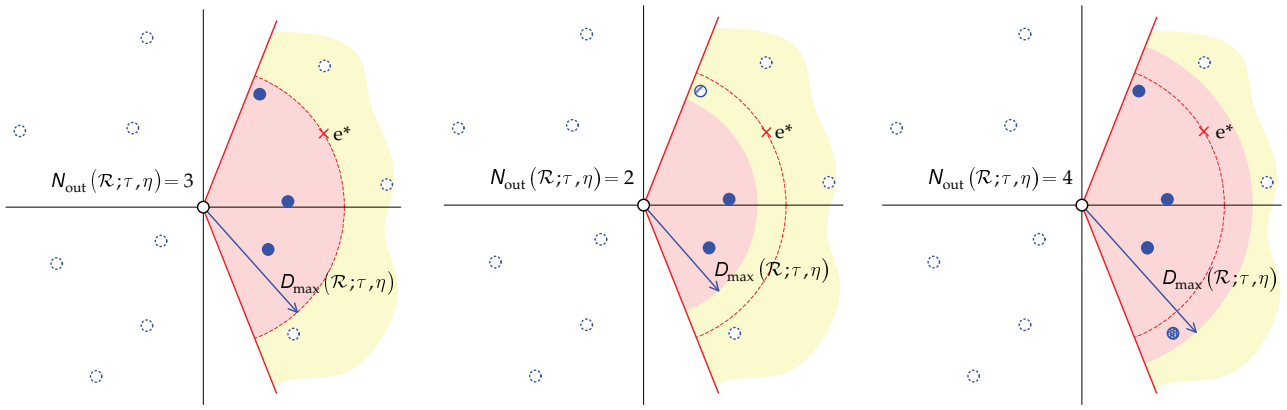

(a) $\eta = 1$ (b) $\eta < 1$ (c) $\eta > 1$

Fig. 2. Secrecy range $D_{\max}(\mathcal{R};\tau,\eta)$ and out-degree $N_{\text{out}}(\mathcal{R};\tau,\eta)$ of the probe transmitter for three cases: (a) $\eta = 1$, (b) $\eta < 1$, and (c) $\eta > 1$.

the probe transmitter with knowing the location information of eavesdroppers is most adversarial in (34). Hence, using the Shannon transform of the Marčenko–Pastur law $f^{\star}(z;\tau)$ [55], we get

$$\mathcal{R}_{\text{s}}^{\star}(x,\Omega,\tau,\eta) = \left[\mathcal{V}\left(\frac{\gamma}{\tau|x|^{\alpha}},\tau\right) - \frac{1}{\eta}\mathcal{V}\left(\frac{\gamma}{\eta\tau|e^{\star}|^{\alpha}},\eta\tau\right)\right]^{+} \tag{36}$$

where

$$e^{\star} = \arg\min_{e\in\Pi_{\text{e}}\cap\mathcal{R}} |e| \tag{37}$$

and

$$\begin{aligned}\mathcal{V}(x,y) &\triangleq \int_{a_y}^{b_y} \ln(1+xz)\, f^{\star}(z;y)\, dz \\ &= y\ln(1+x-\mathcal{F}(x,y)) \\ &\quad + \ln(1+xy-\mathcal{F}(x,y)) - \frac{1}{x}\mathcal{F}(x,y)\end{aligned} \tag{38}$$

with

$$\mathcal{F}(x,y) = \frac{1}{4}\left(\sqrt{x(1+\sqrt{y})^2+1} - \sqrt{x(1-\sqrt{y})^2+1}\right)^2. \tag{39}$$

Proposition 5 (Space–Time Secrecy Rate in Poisson Fields): Let $\Psi = \Pi_{\text{r}}$ and $\Omega = \Pi_{\text{e}}$. Then, the space–time secrecy rate in nats/s/Hz into $\mathcal{R} = \mathcal{S}(\phi,\infty)$ is given by (40).

Proof: It follows from (36), Campbell's theorem, and the fact that $|e^{\star}| \sim \text{Rayleigh}\left(1/\sqrt{2\lambda_{\text{e}}\phi}\right)$. □

Remark 8: As $\eta \to \infty$, the eavesdropping capacity per receive antenna (the second term) in (36) goes to zero and hence, we have

$$i\mathcal{S}(\mathcal{R};\tau,\infty) = \frac{\Delta_{\text{r}}}{\Delta_{\text{s}}}\mathcal{C}^{\star}(\mathcal{R};\tau). \tag{41}$$

This unveils that there exists a secrecy code which guarantees that the eavesdroppers get no information as the growing rate of n_{r} increases and/or that of n_{e} decreases.

E. Local Confidential Connectivity

1) Secrecy Range: The range $D_{\max}(\mathcal{R};\tau,\eta)$ of confidential connection with a positive secrecy rate, called the *secrecy range*, is the maximum *feasible* length of edges in the local secrecy graph $\mathcal{G}(\mathcal{R})$, which is the solution of

$$\mathcal{V}\left(\frac{\gamma}{\tau D_{\max}^{\alpha}(\mathcal{R};\tau,\eta)},\tau\right) = \frac{1}{\eta}\mathcal{V}\left(\frac{\gamma}{\eta\tau|e^{\star}|^{\alpha}},\eta\tau\right). \tag{42}$$

The legitimate receiver $x \in \Psi$ in $\mathcal{R}$ with the distance (from the transmitter) $|x|$ less than $D_{\max}(\mathcal{R};\tau,\eta)$ achieves a positive secrecy rate, belonging to the local secrecy graph $\mathcal{G}(\mathcal{R})$. Note that the secrecy range depends only on the spatial distribution of eavesdroppers and the limiting ratios τ and η. When $\eta = 1$ (the antenna numbers of the receiver and eavesdropper grow at the same rate), the solution of (42) simply becomes $D_{\max}(\mathcal{R};\tau,1) = |e^{\star}|$ independent of τ. Hence, the secrecy range is equal to the nearest eavesdropper distance, which is distributed as $D_{\max}(\mathcal{R};\tau,1) \sim \text{Rayleigh}\left(1/\sqrt{2\lambda_{\text{e}}\phi}\right)$ with the average secrecy range

$$\langle D_{\max}(\mathcal{R};\tau,1)\rangle = \frac{1}{2}\sqrt{\frac{\pi}{\lambda_{\text{e}}\phi}} \tag{43}$$

for $\Omega = \Pi_{\text{e}}$ and $\mathcal{R} = \mathcal{S}(\phi,\infty)$.

2) Out-Degree: The out-degree $N_{\text{out}}(\mathcal{R};\tau,\eta)$ of the probe transmitter in the local graph $\mathcal{G}(\mathcal{R})$ is defined as the cardi-

$$i\mathcal{S}(\mathcal{R};\tau,\eta) = \frac{4\lambda_{\text{r}}\lambda_{\text{e}}\phi^2}{\Delta_{\text{s}}}\int_0^{\infty}\int_0^{\infty} rz\left[\mathcal{V}\left(\frac{\gamma}{\tau r^{\alpha}},\tau\right) - \frac{1}{\eta}\mathcal{V}\left(\frac{\gamma}{\eta\tau z^{\alpha}},\eta\tau\right)\right]^{+} e^{-\lambda_{\text{e}}\phi z^2} dr dz \tag{40}$$

nality of the edge set $\mathcal{E}$ or equivalently,

$$\begin{aligned} &N_{\text{out}}\left(\mathcal{R};\tau,\eta\right) \\ &\quad=\sum_{x\in\Psi\cap\mathcal{R}}\mathbb{1}\left\{\mathcal{V}\left(\frac{\gamma}{\tau\left|x\right|^{\alpha}},\tau\right)>\frac{1}{\eta}\mathcal{V}\left(\frac{\gamma}{\eta\tau\left|e^{\star}\right|^{\alpha}},\eta\tau\right)\right\} \\ &\quad=\sum_{x\in\Psi\cap\mathcal{R}}\mathbb{1}\Big\{\left|x\right|<D_{\max}\left(\mathcal{R};\tau,\eta\right)\Big\}. \end{aligned} \tag{44}$$

As illustrated in Fig. 2, the out-degree $N_{\text{out}}\left(\mathcal{R};\tau,\eta\right)$ of the probe transmitter depends on the secrecy range $D_{\max}\left(\mathcal{R};\tau,\eta\right)$ that is smaller than the nearest eavesdropper distance $\left|e^{\star}\right|$ if $\eta<1$; equal to $\left|e^{\star}\right|$ if $\eta=1$; and larger than $\left|e^{\star}\right|$ if $\eta>1$. In fact, the out-degree $N_{\text{out}}\left(\mathcal{R};\tau,\eta\right)$ is equal to the number of legitimate receivers sitting in $\mathcal{S}\left(\phi,D_{\max}\left(\mathcal{R};\tau,\eta\right)\right)$. In a symmetric antenna configuration ($\eta=1$) Fig. 2(a), the out-degree is characterized simply by a geometric distance of the nearest eavesdropper, which captures the dominant information leakage. However, in asymmetric antenna configurations Fig. 2(b) and 2(c), the out-degree is changeable as η (and hence, $D_{\max}\left(\mathcal{R};\tau,\eta\right)$) varies.

For $\Psi=\Pi_{\text{r}}$, $\Omega=\Pi_{\text{e}}$, and $\mathcal{R}=\mathcal{S}\left(\phi,\infty\right)$, the out-degree $N_{\text{out}}\left(\mathcal{R};\tau,\eta\right)$ given $D_{\max}\left(\mathcal{R};\tau,\eta\right)=r$ is equal to the number of legitimate receivers sitting in $\mathcal{S}\left(\phi,r\right)$, which is distributed as a Poisson variable:

$$\begin{aligned} &\mathbb{P}\left\{N_{\text{out}}\left(\mathcal{R};\tau,\eta\right)=k|D_{\max}\left(\mathcal{R};\tau,\eta\right)=r\right\} \\ &\qquad=e^{-\lambda_{\text{r}}\phi r^{2}}\frac{\left(\lambda_{\text{r}}\phi r^{2}\right)^{k}}{k!},\qquad k\in\mathbb{Z}_{+}. \end{aligned} \tag{45}$$

Therefore, the average out-degree $\left\langle N_{\text{out}}\left(\mathcal{R};\tau,\eta\right)\right\rangle$ is given by

$$\begin{aligned} \left\langle N_{\text{out}}\left(\mathcal{R};\tau,\eta\right)\right\rangle &=\mathbb{E}\left\{\mathbb{E}\left\{N_{\text{out}}\left(\mathcal{R};\tau,\eta\right)|D_{\max}\left(\mathcal{R};\tau,\eta\right)\right\}\right\} \\ &=\lambda_{\text{r}}\phi\,\mathbb{E}\left\{D_{\max}^{2}\left(\mathcal{R};\tau,\eta\right)\right\}. \end{aligned} \tag{46}$$

For the symmetric case $\eta=1$, (46) reduces to

$$\left\langle N_{\text{out}}\left(\mathcal{R};\tau,1\right)\right\rangle=\frac{\lambda_{\text{r}}}{\lambda_{\text{e}}} \tag{47}$$

which is independent of τ and exactly equal to the spatial density ratio between the legitimate receivers and eavesdroppers.

Remark 9: By setting the multicast degree of freedom to $\Delta_{\text{s}}=\left\langle N_{\text{out}}\left(\mathcal{R};\tau,\eta\right)\right\rangle$, we can evaluate the sum secrecy rate for multicasting to the legitimate receivers within the average secrecy range with uniform scheduling in Proposition 5.

3) Out-Isolation: The out-isolation of the probe transmitter in the local graph $\mathcal{G}\left(\mathcal{R}\right)$ occurs if the transmitter is not securely connected to any legitimate receivers in $\mathcal{R}$ or equivalently, the edge set $\mathcal{E}$ is *empty*. Hence, the out-isolation probability $P_{\text{iso}}\left(\mathcal{R};\tau,\eta\right)$ of the probe transmitter in $\mathcal{R}$ is given by

$$\begin{aligned} P_{\text{iso}}\left(\mathcal{R};\tau,\eta\right) &=\mathbb{P}\left\{N_{\text{out}}\left(\mathcal{R};\tau,\eta\right)=0\right\} \\ &=\mathbb{P}\left\{R_{1}>D_{\max}\left(\mathcal{R};\tau,\eta\right)\right\} \\ &=\mathbb{E}\left\{F_{D_{\max}\left(\mathcal{R};\tau,\eta\right)}\left(R_{1}\right)\right\}. \end{aligned} \tag{48}$$

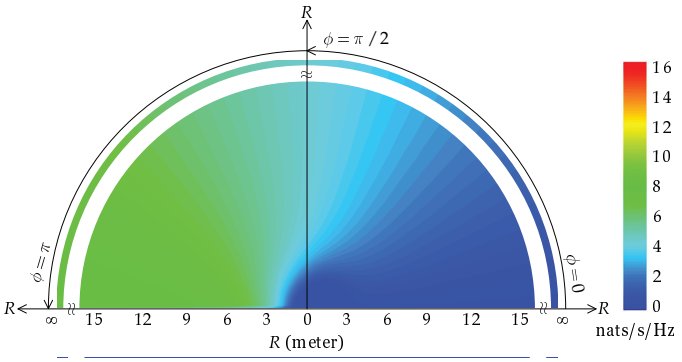

(a) $n_{\text{r}}=n_{\text{t}}=2$

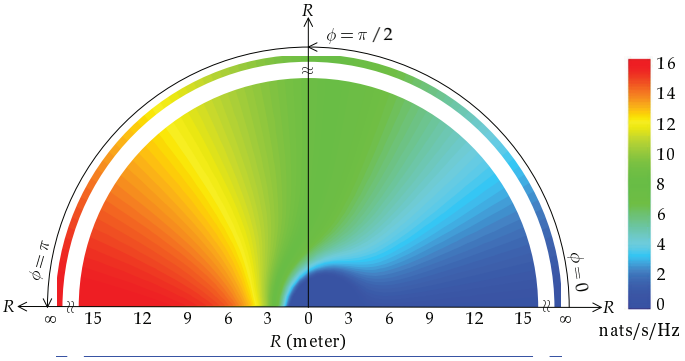

(b) $n_{\text{r}}=n_{\text{t}}=4$

Fig. 3. Space–time capacity $\mathcal{C}\left(\mathcal{R}\right)$ (nats/s/Hz) into $\mathcal{R}=\mathcal{S}\left(\phi,R\right)$ as a function of the sectoring angle ϕ and radius R for (a) $n_{\text{r}}=n_{\text{t}}=2$ and (b) $n_{\text{r}}=n_{\text{t}}=4$ when $\gamma=20$ dB, $\lambda_{\text{r}}=0.01$, and $\alpha=4$.

For $\Psi=\Pi_{\text{r}}$, $\Omega=\Pi_{\text{e}}$, $\mathcal{R}=\mathcal{S}\left(\phi,\infty\right)$, and $\eta=1$, we have

$$P_{\text{iso}}\left(\mathcal{R};\tau,1\right)=\frac{\lambda_{\text{e}}}{\lambda_{\text{r}}+\lambda_{\text{e}}} \tag{49}$$

which is equal to the eavesdropper's fraction of total spatial densities and again independent of the limiting ratio τ. As can be seen from (43), (47), and (49), the use of multiple antennas does not affect secure connectivity if the eavesdroppers have as many antennas as the receiver ($\eta=1$).

IV. Numerical Results

In this section, we provide some numerical examples to demonstrate the characteristics of local (confidential) information flow in Poisson MIMO multicast networks. In all examples, we set: i) the power loss exponent to $\alpha=4$; ii) the sectoral transmission region to $\mathcal{R}=\mathcal{S}\left(\pi/3,\infty\right)$ except Fig. 3; iii) the multicast degrees of freedom to $\Delta_{\text{r}}=\Delta_{\text{s}}=1$; and iv) spatial random fields of legitimate receivers and eavesdroppers to $\Psi=\Pi_{\text{r}}\left(\lambda_{\text{r}}\right)$ and $\Omega=\Pi_{\text{e}}\left(\lambda_{\text{e}}\right)$, respectively.

A. MIMO Multicasting

Fig. 3 shows the space–time capacity $\mathcal{C}\left(\mathcal{R}\right)$ into $\mathcal{R}=\mathcal{S}\left(\phi,R\right)$ as a function of the sectoring angle ϕ and radius R for (a) $n_{\text{r}}=n_{\text{t}}=2$ and (b) $n_{\text{r}}=n_{\text{t}}=4$ when $\gamma=20$ dB and $\lambda_{\text{r}}=0.01$. In contour plots, the colors represent the values of $\mathcal{C}\left(\mathcal{R}\right)$ in nats/s/Hz for the corresponding sectoring angle ϕ and radius R. We observe that $\mathcal{C}\left(\mathcal{R}\right)$ approaches quickly

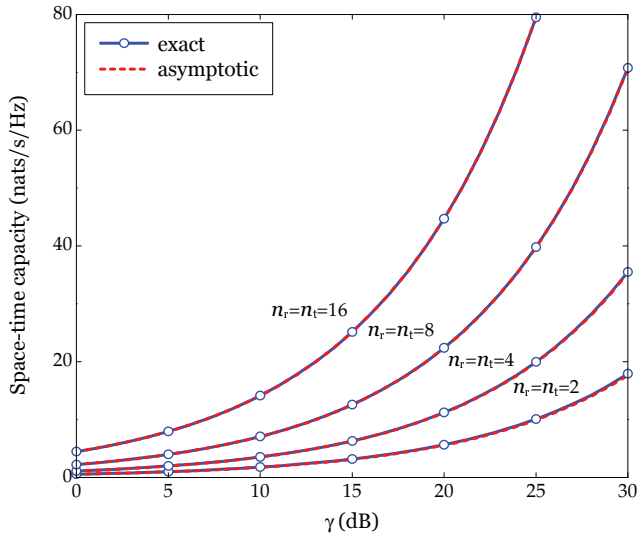

Fig. 4. Space–time capacity $\mathcal{C}(\mathcal{R})$ (nats/s/Hz) and its scaled asymptote $n_{\mathrm{r}}\mathcal{C}^{\star}(\mathcal{R};1)$ into $\mathcal{R}=\mathcal{S}(\pi/3,\infty)$ as a function of γ when $\lambda_{\mathrm{r}}=0.1$, $\alpha=4$, and $n_{\mathrm{r}}=n_{\mathrm{t}}=2$, 4, 8, 16.

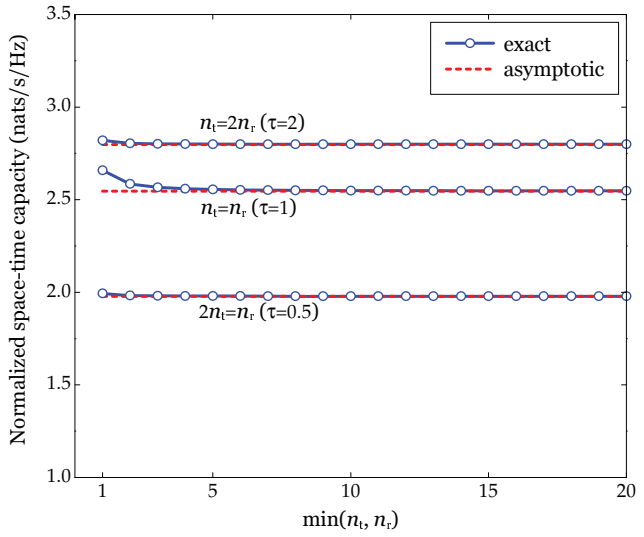

Fig. 5. Normalized space–time capacity $\mathcal{C}(\mathcal{R})/n_{\mathrm{r}}$ (nats/s/Hz) and its asymptote $\mathcal{C}^{\star}(\mathcal{R};\tau)$ into $\mathcal{R}=\mathcal{S}(\pi/3,\infty)$ as a function of $\min(n_{\mathrm{r}},n_{\mathrm{t}})$ for $2n_{\mathrm{t}}=n_{\mathrm{r}}$ ($\tau=0.5$), $n_{\mathrm{t}}=n_{\mathrm{r}}$ ($\tau=1$), and $n_{\mathrm{t}}=2n_{\mathrm{r}}$ ($\tau=2$) when $\gamma=20$ dB, $\lambda_{\mathrm{r}}=0.1$, and $\alpha=4$.

to (11) in Remark 3 as R increases, since the contributions of legitimate receivers far from the transmitter to $\mathcal{C}(\mathcal{R})$ are negligible due to large path losses. To illustrate the scaling of $\mathcal{C}(\mathcal{R})$ with the number of antennas, the space–time capacity $\mathcal{C}(\mathcal{R})$ and its scaled asymptote $n_{\mathrm{r}}\mathcal{C}^{\star}(\mathcal{R};1)$ is depicted in Fig. 4 as a function of γ when $\lambda_{\mathrm{r}}=0.1$ and $n_{\mathrm{r}}=n_{\mathrm{t}}=2$, 4, 8, 16. We see that $\mathcal{C}(\mathcal{R})$ scales with the number of antennas and its asymptotic scaling argument is extremely tight. To further ascertain fast convergence to asymptote, we plot the normalized space–time capacity $\mathcal{C}(\mathcal{R})/n_{\mathrm{r}}$ and its asymptote $\mathcal{C}^{\star}(\mathcal{R};\tau)$ in Fig. 5 as a function of $\min(n_{\mathrm{r}},n_{\mathrm{t}})$ for $2n_{\mathrm{t}}=n_{\mathrm{r}}$ ($\tau=0.5$), $n_{\mathrm{t}}=n_{\mathrm{r}}$ ($\tau=1$), and $n_{\mathrm{t}}=2n_{\mathrm{r}}$ ($\tau=2$) when $\gamma=20$ dB and $\lambda_{\mathrm{r}}=0.1$. Even for two antennas, the asymptotic result gives a remarkably accurate approximation to the exact value.

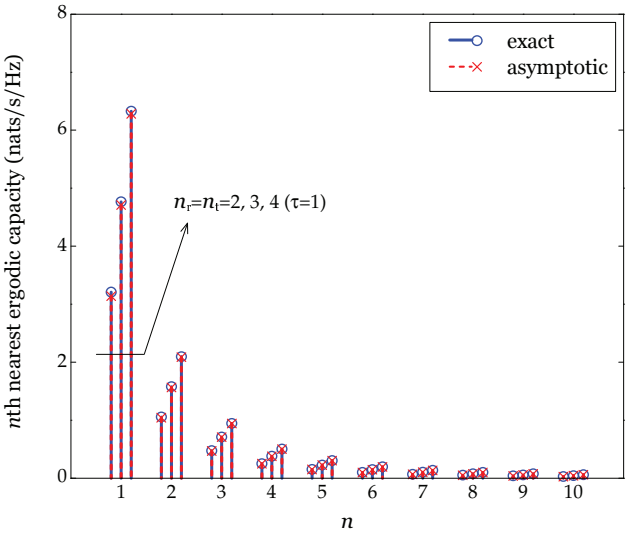

Fig. 6. The nth nearest ergodic capacity $\langle C\rangle_n(\mathcal{R})$ (nats/s/Hz) and its scaled asymptote $n_{\mathrm{r}}C_n^{\star}(\mathcal{R};1)$ in $\mathcal{R}=\mathcal{S}(\pi/3,\infty)$ as a function of n when $\lambda_{\mathrm{r}}=0.1$, $\gamma=20$ dB, $\alpha=4$, and $n_{\mathrm{r}}=n_{\mathrm{t}}=2$, 3, 4 ($\tau=1$).

Fig. 6 shows the nth nearest ergodic capacity $\langle C\rangle_n(\mathcal{R})$ and its scaled asymptote $n_{\mathrm{r}}C_n^{\star}(\mathcal{R};1)$ as a function of n when $\lambda_{\mathrm{r}}=0.1$, $\gamma=20$ dB, and $n_{\mathrm{r}}=n_{\mathrm{t}}=2$, 3, 4 ($\tau=1$). We observe that the nth nearest ergodic capacity decreases exponentially as n increases and the asymptotic analysis predicts the exact value remarkably accurately. To demonstrate the effect of the limiting ratio τ on scaling behavior, the asymptotic space–time capacity $\mathcal{C}^{\star}(\mathcal{R};\tau)$ and the nth nearest asymptotic ergodic capacity $C_n^{\star}(\mathcal{R};\tau)$ per receive antenna are depicted in Fig. 7 as a function of τ when $\gamma=20$ dB, $\lambda_{\mathrm{r}}=0.1$, and $n=1$, 2, 3. As τ grows, $\mathcal{C}^{\star}(\mathcal{R};\tau)$ and $C_n^{\star}(\mathcal{R};\tau)$ are monotonically increasing, until reaching their limits in (27) and (32), respectively: $\mathcal{C}^{\star}(\mathcal{R};\infty)=3.29$ nats/s/Hz and $C_n^{\star}(\mathcal{R};\infty)=1.90$, 0.63, 0.27 nats/s/Hz for $n=1$, 2, 3 in this example. We also see that the nth nearest ergodic capacity for small values of n (e.g., up to the third nearest legitimate receiver) contributes dominantly to the space–time capacity.

B. Secure MIMO Multicasting

Fig. 8 shows the space–time secrecy rate $i\mathcal{S}(\mathcal{R};\tau,\eta)$ as a function of η when $\gamma=20$ dB, $\lambda_{\mathrm{r}}=0.1$, $\lambda_{\mathrm{e}}=0.01$, and $\tau=0.01$, 0.1, 1, 10. For each value of τ, $i\mathcal{S}(\mathcal{R};\tau,\eta)$ is monotonically increasing with η until reaching its limit in (41) equal to the asymptotic space-time capacity at the corresponding τ, whereas not monotonically increasing with τ in general (unlike the asymptotic space–time capacity)—especially when $\eta<1$. In this example, we have $i\mathcal{S}(\mathcal{R};\tau,\infty)=0.33$, 1.03, 2.79, and 3.25 nats/s/Hz for $\tau=0.01$, 0.1, 1, and 10, respectively.

Figs. 9–11 demonstrate the effects of τ and η on local confidential connectivity. The average secrecy range $\langle D_{\max}(\mathcal{R};\tau,\eta)\rangle$ and the average out-degree $\langle N_{\mathrm{out}}(\mathcal{R};\tau,\eta)\rangle$ is depicted in Fig. 9 as a function of η at $\tau=1$, while as a function of τ at $\eta=0.1$ in Fig. 10, when $\gamma=20$ dB, $\lambda_{\mathrm{r}}=0.1$, and $\lambda_{\mathrm{e}}=0.01$. The average secrecy range and out-degree increase with the limiting ratio η due to a more MIMO

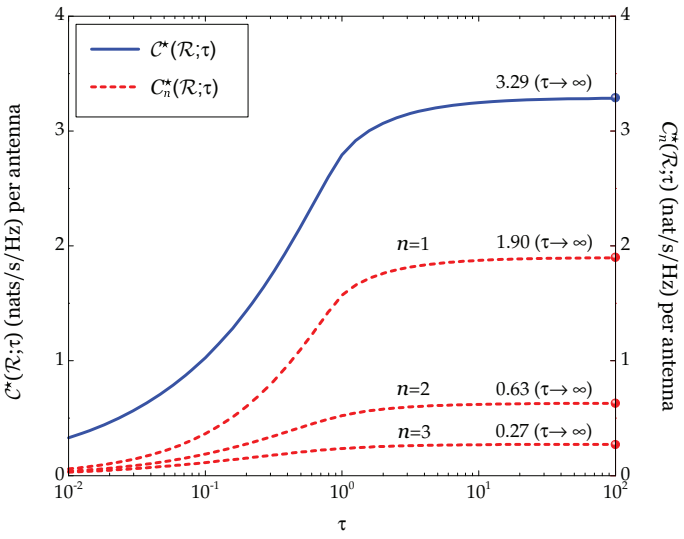

Fig. 7. Asymptotic space–time capacity $\mathcal{C}^\star(\mathcal{R};\tau)$ and nth nearest asymptotic ergodic capacity $C_n^\star(\mathcal{R};\tau)$ in nats/s/Hz per receive antenna into $\mathcal{R} = \mathcal{S}(\pi/3,\infty)$ as a function of τ when $\gamma = 20$ dB, $\lambda_r = 0.1$, $\alpha = 4$, and $n = 1, 2, 3$.

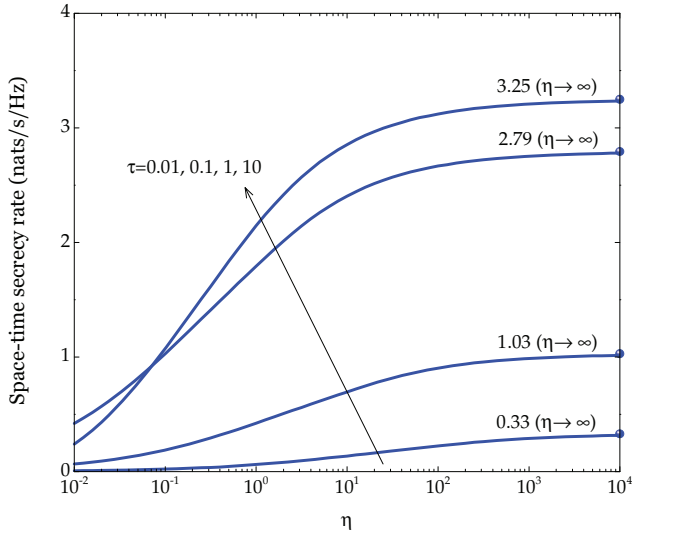

Fig. 8. Space–time secrecy rate $i\mathcal{S}(\mathcal{R};\tau,\eta)$ (nats/s/Hz) into $\mathcal{R} = \mathcal{S}(\pi/3,\infty)$ as a function of η when $\gamma = 20$ dB, $\lambda_r = 0.1$, $\lambda_e = 0.01$, $\alpha = 4$, and $\tau = 0.01, 0.1, 1, 10$.

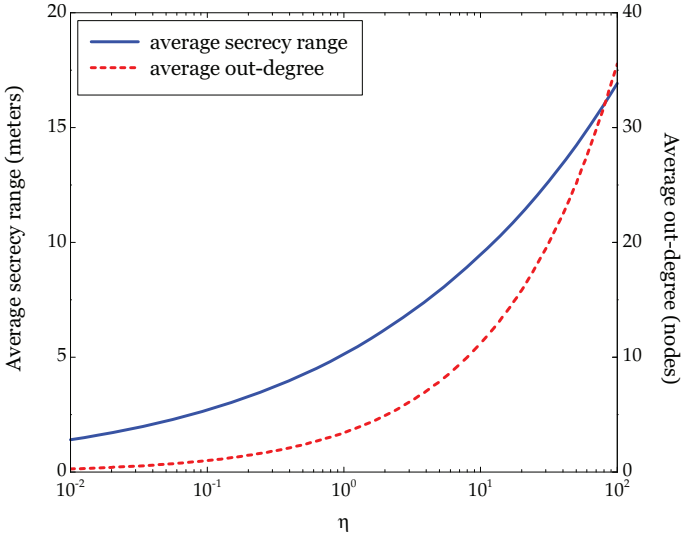

Fig. 9. Average secrecy range $\langle D_{\max}(\mathcal{R};\tau,\eta)\rangle$ and average out-degree $\langle N_{\text{out}}(\mathcal{R};\tau,\eta)\rangle$ in $\mathcal{R} = \mathcal{S}(\pi/3,\infty)$ as a function of η when $\gamma = 20$ dB, $\lambda_r = 0.1$, $\lambda_e = 0.01$, $\alpha = 4$, and $\tau = 1$.

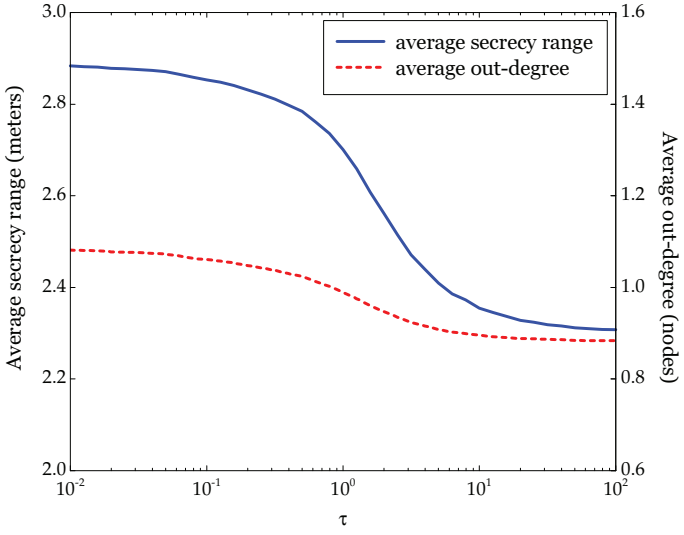

Fig. 10. Average secrecy range $\langle D_{\max}(\mathcal{R};\tau,\eta)\rangle$ and average out-degree $\langle N_{\text{out}}(\mathcal{R};\tau,\eta)\rangle$ in $\mathcal{R} = \mathcal{S}(\pi/3,\infty)$ as a function of τ when $\gamma = 20$ dB, $\lambda_r = 0.1$, $\lambda_e = 0.01$, $\alpha = 4$, and $\eta = 0.1$.

gain in the legitimate links than the eavesdropper link, whereas the effect of τ on these measures of confidential connectivity depends on a regime of η. When $\eta < 1$, $\langle D_{\max}(\mathcal{R};\tau,\eta)\rangle$ and $\langle N_{\text{out}}(\mathcal{R};\tau,\eta)\rangle$ decrease as τ increases (see Fig. 10), while increasing with τ if $\eta > 1$ and not varying with τ if $\eta = 1$ as shown in (43) and (47). We also see from Fig. 9 and Fig. 10 that the effects of η on $\langle D_{\max}(\mathcal{R};\tau,\eta)\rangle$ and $\langle N_{\text{out}}(\mathcal{R};\tau,\eta)\rangle$ are more pronounced than those of τ. Finally, Fig. 11 shows the out-isolation probability $P_{\text{iso}}(\mathcal{R};\tau,\eta)$ as a function of η when $\gamma = 20$ dB, $\lambda_r = 0.1$, $\lambda_e = 0.01$, and $\tau = 0.1, 1, 10$. We can make the same observations on the impacts of τ and η to $P_{\text{iso}}(\mathcal{R};\tau,\eta)$ as observed on the average secrecy range and out-degree in Fig. 9 and Fig. 10.

V. Conclusion

Using key results of stochastic geometry and random matrix theory, we developed a framework to characterize multicasting in stochastic MIMO networks. A transmitter located at the origin broadcasts confidential data with sectorized transmission into a region $\mathcal{R}$, while legitimate receivers and eavesdroppers are scattered randomly according to homogeneous PPPs in space. Without accounting for communication confidentiality at the physical layer, we analyzed the space–time capacity to measure a total information flow into $\mathcal{R}$ and the nth nearest ergodic capacity to characterize the spatial ordering of MIMO ergodic capacity achieved by legitimate receivers in $\mathcal{R}$. We further determined the asymptotic space–time capacity and the nth nearest ergodic capacity as the antenna numbers tend to infinity. It has been shown that i) a few nearest legitimate receivers from the probe transmitter play a part in the total in-

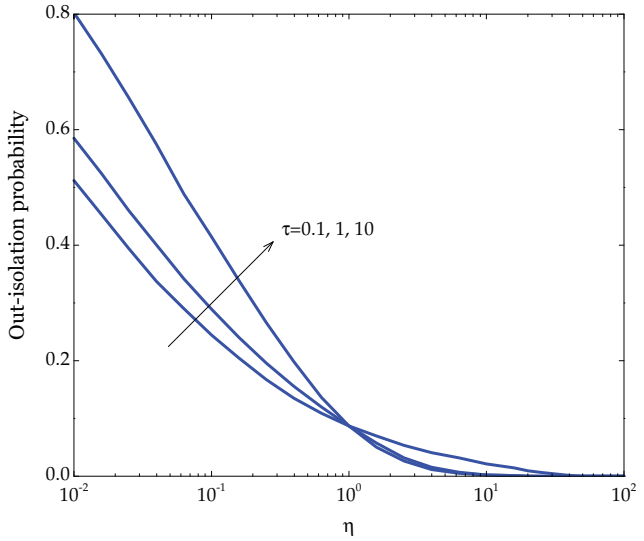

Fig. 11. Out-isolation probability $P_{\rm iso}\left(\mathcal{R};\tau,\eta\right)$ in $\mathcal{R}=\mathcal{S}\left(\pi/3,\infty\right)$ as a function of η when $\gamma=20$ dB, $\lambda_{\rm r}=0.1$, $\lambda_{\rm e}=0.01$, $\alpha=4$, and $\tau=0.1$, 1, 10.

formation flow into $\mathcal{R}$; and ii) the asymptotic analysis provides striking accuracy in predicting the exact result even for two antennas. In the presence of eavesdroppers, we determined a total amount of confidential information flow per receive antenna, named the space–time secrecy rate, into $\mathcal{R}$ with asymptotic arguments. Using the asymptotic secrecy graph on $\mathcal{R}$, we also characterized local confidential connectivity such as the secrecy range, out-degree, and out-isolation probability of the probe transmitter.

REFERENCES

[1] 3GPP, "Multimedia broadcast/multicast service (MBMS) user service guidelines," TR 26.946 (Release 10), 2011.

[2] ——, "Security of multimedia broadcast/multicast service (MBMS)," TS 33.246 (Release 10), 2011.

[3] T. Jiang, W. Xiang, H.-H. Chen, and Q. Ni, "Multicast broadcast services support in OFDMA-based WiMAX systems," *IEEE Commun. Mag.*, vol. 8, no. 45, pp. 78–86, Aug. 2007.

[4] H. Won, H. Cai, D. Y. Eun, K. Guo, A. Netravali, I. Rhee, and K. Sabnani, "Multicast scheduling in cellular data networks," *IEEE Trans. Wireless Commun.*, vol. 8, no. 9, pp. 4540–4549, Sept. 2009.

[5] C.-H. Liu and J. G. Andrews, "Multicast outage probability and transmission capacity of multihop wireless networks," *IEEE Trans. Inf. Theory*, vol. 57, no. 7, pp. 4344–4358, July 2011.

[6] P. K. Gopala and H. E. Gamal, "Opportunistic multicasting," in *Proc. 2004 IEEE Asilomar Conf. Signals, Syst. Comput.*, pp. 845–849.

[7] ——, "Scheduling for cellular multicast: a cross-layer perspective," *IEEE Trans. Mobile Comput.*, submitted for publication.

[8] T.-P. Low, M.-O. Pun, Y.-W. P. Hong, and C.-C. J. Kuo, "Optimized opportunistic multicast scheduling (OMS) over wireless cellular networks," *IEEE Trans. Wireless Commun.*, vol. 9, no. 2, pp. 791–801, Feb. 2010.

[9] C. Suh and J. Mo, "Resource allocation for multicast services in multicarrier wireless communications," *IEEE Trans. Wireless Commun.*, vol. 7, no. 1, pp. 27–31, Jan. 2008.

[10] S. Lakshminarayana and A. Eryilmaz, "Multirate multicasting with interlayer network coding," *IEEE/ACM Trans. Netw.*, to be published.

[11] N. D. Sidiropoulos, T. N. Davidson, and Z.-Q. T. Luo, "Transmit beamforming for physical-layer multicasting," *IEEE Trans. Signal Process.*, vol. 54, no. 6, pp. 2239–2251, June 2006.

[12] A. Abdelkader, A. B. Gershman, and N. D. Sidiropoulos, "Multiple-antenna multicasting using channel orthogonalization and local refinement," *IEEE Trans. Signal Process.*, vol. 58, no. 7, pp. 3922–3927, June 2010.

[13] R. F. Wyrembelski, T. J. Oechtering, and H. Boche, "MIMO Gaussian bidirectional broadcast channels with common messages," *IEEE Trans. Inf. Theory*, vol. 10, no. 9, pp. 2950–2959, Sept. 2011.

[14] Y. Huang, Q. Li, W.-K. Ma, and S. Zhang, "Robust multicast beamforming for spectrum sharing-based cognitive radios," *IEEE Trans. Signal Process.*, vol. 60, no. 1, pp. 527–533, Jan. 2012.

[15] E. Chiu and V. K. N. Lau, "Precoding design for multi-antenna multicast broadcast services with limited feedback," *IEEE Syst. J.*, vol. 4, no. 4, pp. 550–560, Dec. 2010.

[16] J. Wolf, A. Wyner, and J. Ziv, "Source coding for multiple descriptions," *Bell Syst. Tech. J.*, vol. 59, no. 8, pp. 1417–1426, Oct. 1980.

[17] W. K. Goyal, "Multiple description coding: compression meets the network," *IEEE Signal Process. Mag.*, vol. 18, no. 5, pp. 74–93, Sept. 2001.

[18] M. Effros, "Universal multiresolution source codes," *IEEE Trans. Inf. Theory*, vol. 47, no. 6, pp. 2113–2129, Sept. 2001.

[19] Wireless LAN Medium Access Control (MAC) and Physical Layer (PHY) Specifications—Amendment 5: Enhancements for Higher Throughput, IEEE Std. 802.11n, Oct. 2009.

[20] Air Interface for Broadband Wireless Access Systems, IEEE Std. 802.16, May 2009.

[21] Evolved Universal Terrestrial Radio Access (EUTRA) and Evolved Universal Terrestrial Radio Access Network (EUTRAN): Overall Description, 3GPP Std. TS 36.300, V8.9.0, May 2009.

[22] Requirements for Further Advancements for Evolved Universal Terrestrial Radio Access (E-UTRA) (LTE-Advanced), 3GPP Std. TR 36. 913, V9.0.0, Dec. 2009.

[23] H. Shin and J. H. Lee, "Capacity of multiple-antenna fading channels: spatial fading correlation, double scattering, and keyhole," *IEEE Trans. Inf. Theory*, vol. 49, no. 10, pp. 2636–2647, Oct. 2003.

[24] M. Chiani, M. Z. Win, and A. Zanella, "On the capacity of spatially correlated MIMO Rayleigh-fading channels," *IEEE Trans. Inf. Theory*, vol. 49, no. 10, pp. 2363–2371, Oct. 2003.

[25] H. Shin, M. Z. Win, J. H. Lee, and M. Chiani, "On the capacity of doubly correlated MIMO channels," *IEEE Trans. Wireless Commun.*, vol. 5, no. 8, pp. 2253–2265, Aug. 2006.

[26] M. Chiani, M. Z. Win, and H. Shin, "MIMO networks: the effects of interference," *IEEE Trans. Inf. Theory*, vol. 56, no. 1, pp. 336–349, Jan. 2010.

[27] C.-N. Chuah, D. N. C. Tse, J. M. Kahn, and R. A. Valenzuela, "Capacity scaling in MIMO wireless systems under correlated fading," *IEEE Trans. Inf. Theory*, vol. 48, no. 3, pp. 637–650, Mar. 2002.

[28] H. Shin, M. Z. Win, and M. Chiani, "Asymptotic statistics of mutual information for doubly correlated MIMO channels," *IEEE Trans. Wireless Commun.*, vol. 7, no. 2, pp. 562–573, Feb. 2008.

[29] H. Shin and M. Z. Win, "MIMO diversity in the presence of double scattering," *IEEE Trans. Inf. Theory*, vol. 54, no. 7, pp. 2976–2996, July 2008.

[30] ——, "Gallager's exponent for MIMO channels: a reliability–rate tradeoff," *IEEE Trans. Commun.*, vol. 57, no. 4, pp. 972–985, Apr. 2009.

[31] Y. Jeong, H. Shin, and M. Z. Win, "Superanalysis of optimum combining with application to femtocell networks," *IEEE J. Sel. Areas Commun.*, vol. 30, no. 3, pp. 509–524, Apr. 2012.

[32] C. E. Shannon, "Communication theory of secrecy systems," *Bell Syst. Tech. J.*, vol. 28, pp. 656–715, Oct. 1949.

[33] A. D. Wyner, "The wire-tap channel," *Bell Syst. Tech. J.*, vol. 54, pp. 1355–1387, Oct. 1975.

[34] M. Bloch, J. Barros, M. R. D. Rodrigues, and S. W. McLaughlin, "Wireless information-theoretic security," *IEEE Trans. Inf. Theory*, vol. 54, no. 6, pp. 2515–2534, June 2008.

[35] A. Khisti and G. W. Wornell, "Secure transmission with multiple antennas—part I: the MISOME wiretap channel," *IEEE Trans. Inf. Theory*, vol. 56, no. 7, pp. 3088–3104, July 2010.

[36] ——, "Secure transmission with multiple antennas—part II: the MIMOME wiretap channel," *IEEE Trans. Inf. Theory*, vol. 56, no. 11, pp. 5515–5532, Nov. 2010.

[37] F. Oggier and B. Hassibi, "The secrecy capacity of the MIMO wiretap channel," *IEEE Trans. Inf. Theory*, vol. 57, no. 8, pp. 4961–4972, 2011.

[38] M. Yuksel and E. Erkip, "Diversity-multiplexing tradeoff for the multiple-antenna wire-tap channel," *IEEE Trans. Wireless Commun.*, vol. 10, no. 3, pp. 762–771, Mar. 2011.

[39] T. V. Nguyen and H. Shin, "Power allocation and achievable secrecy rates in MISOME wiretap channels," *IEEE Commun. Lett.*, vol. 15, no. 11, pp. 1196–1198, Nov. 2011.

[40] T. Liu and S. Shamai, "A note on the secrecy capacity of the multiple-antenna wiretap channel," *IEEE Trans. Inf. Theory*, vol. 55, no. 6, pp. 2547–2553, June 2009.

[41] X. He and A. Yener, "Providing secrecy when the eavesdropper channel is arbitrarily varying: a case for multiple antennas," in *Proc. 2010 Allerton Conf. Commun., Control Compu.*, pp. 1228–1235.

[42] J. Kingman, *Poisson Processes*. Oxford University Press, 1993.

[43] D. Stoyan, W. Kendall, and J. Mecke, *Stochastic Geometry and Its Applications*, 2nd ed. John Wiley and Sons, 1996.
[44] J. Orriss and S. K. Barton, "Probability distributions for the number of radio transceivers which can communicate with one another," *IEEE Trans. Commun.*, vol. 51, no. 4, pp. 676–681, Apr. 2003.
[45] P. C. Pinto, A. Giorgetti, M. Z. Win, and M. Chiani, "A stochastic geometry approach to coexistence in heterogeneous wireless networks," *IEEE J. Sel. Areas Commun.*, vol. 27, no. 7, pp. 1268–1282, Sept. 2009.
[46] M. Haenggi, J. G. Andrews, F. Baccelli, O. Dousse, and M. Franceschetti, "Stochastic geometry and random graphs for the analysis and design of wireles networks," *IEEE J. Sel. Areas Commun.*, vol. 27, no. 7, pp. 1029–1046, Sept. 2009.
[47] A. Rabbachin, T. Q. S. Quek, H. Shin, and M. Z. Win, "Cognitive network interference," *IEEE J. Sel. Areas Commun.*, vol. 29, no. 2, pp. 480–493, Feb. 2011.
[48] W. C. Cheung, T. Q. S. Quek, and M. Kountouris, "Throughput optimization, spectrum allocation, and access control in two-tier femtocell networks," *IEEE J. Sel. Areas Commun.*, vol. 30, no. 3, pp. 561–574, Apr. 2012.
[49] E. Salbaroli and A. Zanella, "Interference analysis in a Poisson field of nodes of finite area," *IEEE Trans. Veh. Technol.*, vol. 58, no. 4, pp. 1776–1783, May 2009.
[50] M. Z. Win, P. C. Pinto, and L. A. Shepp, "A mathematical theory of network interference and its applications," *Proc. IEEE*, vol. 97, no. 2, pp. 205–230, Feb. 2009.
[51] P. C. Pinto, J. Barros, and M. Z. Win, "Secure communication in stochastic wireless networks—part I: connectivity," *IEEE Trans. Inf. Forensics Security*, vol. 7, no. 1, pp. 125–138, Feb. 2012.
[52] ——, "Secure communication in stochastic wireless networks—part II: maxmimum rate and collusion," *IEEE Trans. Inf. Forensics Security*, vol. 7, no. 1, pp. 139–147, Feb. 2012.
[53] K. Huang, V. K. N. Lau, and Y. Chen, "Spectrum sharing between cellular and mobile ad hoc networks: transmission-capacity trade-off," *IEEE J. Sel. Areas Commun.*, vol. 27, no. 7, pp. 1256–1267, Sept. 2009.
[54] V. A. Marčenko and L. A. Pastur, "Distribution of eigenvalues for some sets of random matrices," *Math. USSR-Sb*, vol. 1, no. 4, pp. 487–483, 1967.
[55] A. M. Tulino and S. Verdú, "Random matrix theory and wireless communications," *Foundations Trends Commun. Inf. Theory*, vol. 1, no. 1, pp. 1–182, June 2004.
[56] I. S. Gradshteyn and I. M. Ryzhik, *Table of Integrals, Series, and Products*, 7th ed. Academic, 2007.
[57] A. P. Prudnikov, Y. A. Brychkov, and O. I. Marichev, *Integrals and Series*. Gordon and Breach Science, 1990, vol. 3.
[58] A. M. Mathai and R. K. Saxena, *The H-Function with Applications in Statistics and Other Disciplines*. Wiley, 1978.
[59] R. Ramanathan, J. Redi, C. Santivanez, D. Wiggins, and S. Polit, "Ad hoc networking with directional antennas: a complete system solution," *IEEE J. Sel. Areas Commun.*, vol. 23, no. 3, pp. 496–506, Mar. 2005.
[60] A. M. Mathai, R. K. Saxena, and H. J. Haubold, *The H-Function: Theory and Applications*. Springer, 2010.

Youngmin Jeong (S'09) received the B.E. and M.E. degrees in Electronics and Radio Engineering from Kyung Hee University, Yongin, Korea, in 2009 and 2011, respectively. He is currently working toward the Ph.D. degree in Electronics and Radio Engineering at Kyung Hee University. His current research interests include wireless communications, cooperative communications, and heterogeneous networks.

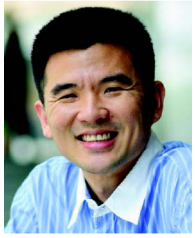

Tony Q.S. Quek (S'98-M'08-SM'12) received the B.E. and M.E. degrees in Electrical and Electronics Engineering from Tokyo Institute of Technology, Tokyo, Japan, respectively. At Massachusetts Institute of Technology (MIT), Cambridge, MA, he earned the Ph.D. in Electrical Engineering and Computer Science. Currently, he is an Assistant Professor with the Information Systems Technology and Design Pillar at Singapore University of Technology and Design (SUTD). He is also a Scientist with the Institute for Infocomm Research. His main research interests are the application of mathematical, optimization, and statistical theories to communication, networking, signal processing, and resource allocation problems. Specific current research topics include cooperative networks, heterogeneous networks, green communications, smart grid, wireless security, compressed sensing, big data processing, and cognitive radio.

Dr. Quek has been actively involved in organizing and chairing sessions, and has served as a member of the Technical Program Committee as well as symposium chairs in a number of international conferences. He is currently an Editor for the IEEE TRANSACTIONS ON COMMUNICATIONS, the IEEE WIRELESS COMMUNICATIONS LETTERS, and an Executive Editorial Committee Member for the IEEE TRANSACTIONS ON WIRELESS COMMUNICATIONS. He was Guest Editor for the *IEEE Communications Magazine* (Special Issue on Heterogeneous and Small Cell Networks) in 2013 and *IEEE Signal Processing Magazine* (Special Issue on Signal Processing for the 5G Revolution) in 2014.

Dr. Quek was honored with the 2008 Philip Yeo Prize for Outstanding Achievement in Research, the IEEE Globecom 2010 Best Paper Award, the 2011 JSPS Invited Fellow for Research in Japan, the CAS Fellowship for Young International Scientists in 2011, the 2012 IEEE William R. Bennett Prize, and the IEEE SPAWC 2013 Best Student Paper Award.

Jin Sam Kwak (S'98-M'04) received his B.S. M.S. and Ph.D. degrees in Electrical Engineering and Computer Science from Seoul National University, Seoul, Korea, in 1998, 2000, and 2004, respectively. From 2004 to 2005, he was a postdoctoral research associate in the School of Electrical and Computer Engineering, Georgia Institute of Technology. During 2006, he was also with the Wireless Networks and Communications Group (WNCG), the University of Texas at Austin as a post-doctoral research fellow. From 2007 to 2012, he was with LG Electronics as a chief research engineer. During this time, he carried out research tasks focused on the IMT-Advanced and its beyond, and also led the standards activities for wireless communications such as IEEE 802 (especially, IEEE 802.11/15/16/19), Wi-Fi Alliance, and WiMAX Forum, as well as served as an alternative board member in Wi-Fi Alliance. Since 2013, he has been with WCS Lab., Korea Advanced Institute of Science and Technology (KAIST) as an adjunct research fellow and also with WILUS Institute of Standards and Technology, where he is currently CEO and co-founder. His main research interests focus on wireless communications and related standards including advanced PHY/MAC technologies for B4G, LTE(-Advanced), and Wi-Fi applications as well as enabling technologies for 5G, IoT/IoE, WPT.

Hyundong Shin (S'01-M'04-SM'11) received the B.S. degree in Electronics Engineering from Kyung Hee University, Korea, in 1999, and the M.S. and Ph.D. degrees in Electrical Engineering from Seoul National University, Seoul, Korea, in 2001 and 2004, respectively. During his postdoctoral research at the Massachusetts Institute of Technology (MIT) from 2004 to 2006, he was with the Wireless Communication and Network Sciences Laboratory within the Laboratory for Information Decision Systems (LIDS).

In 2006, Dr. Shin joined Kyung Hee University, Korea, where he is now an Associate Professor at the Department of Electronics and Radio Engineering. His research interests include wireless communications and information theory with current emphasis on MIMO systems, cooperative and cognitive communications, network interference, vehicular communication networks, location-aware radios and networks, physical-layer security, molecular communications.

Dr. Shin was honored with the Knowledge Creation Award in the field of Computer Science from Korean Ministry of Education, Science and Technology (2010). He received the IEEE Communications Society's Guglielmo Marconi Prize Paper Award (2008) and William R. Bennett Prize Paper Award (2012). He served as a Technical Program Co-chair for the IEEE WCNC (2009 PHY Track) and the IEEE Globecom (Communication Theory Symposium, 2012). He was an Editor for IEEE TRANSACTIONS ON WIRELESS COMMUNICATIONS (2007-2012). He is currently an Editor for IEEE COMMUNICATIONS LETTERS.